

FEW-CYCLE OPTICAL ROGUE WAVES: COMPLEX MODIFIED KORTEWEG-DE VRIES EQUATION

JINGSONG HE^{†*}, LIHONG WANG[†], LINJING LI[†], K.PORSEZIAN[‡] AND R. ERDÉLYI[§]

[†] *Department of Mathematics, Ningbo University, Ningbo, Zhejiang 315211, P. R. China*

[‡] *Department of Physics, Pondicherry University, Pondicherry-605014, India*

[§] *Solar Physics and Space Plasma Research Centre, University of Sheffield, Sheffield, S3 7RH, UK*

ABSTRACT. In this paper, we consider the complex modified Korteweg-de Vries (mKdV) equation as a model of few-cycle optical pulses. Using the Lax pair, we construct a generalized Darboux transformation and systematically generate the first-, second- and third-order rogue wave solutions and analyze the nature of evolution of higher-order rogue waves in detail. Based on detailed numerical and analytical investigations, we classify the higher-order rogue waves with respect to their intrinsic structure, namely, fundamental pattern, triangular pattern, and ring pattern. We also present several new patterns of the rogue wave according to the standard and non-standard decomposition. The results of this paper explain the generalization of higher-order rogue waves in terms of rational solutions. We apply the contour line method to obtain the analytical formulas of the length and width of the first-order RW of the complex mKdV and the NLS equations. In nonlinear optics, the higher-order rogue wave solutions found here will be very useful to generate high-power few-cycle optical pulses which will be applicable in the area of ultra-short pulse technology.

Keywords: complex MKdV equation, Darboux transformation, rogue wave.

PACS number(s): 05.45.Yv, 42.65.Tg, 03.75.Lm, 87.14.gk

1. INTRODUCTION

The theory of nonlinear dynamics has attracted considerable interest and is fundamentally linked to several basic developments in the area of soliton theory. It is well-known that the Korteweg-de Vries (KdV) equation, modified Korteweg-de Vries (mKdV) equation, sine Gordon equation and the nonlinear Schrödinger (NLS) equation are the most typical and well-studied integrable evolution equations which describe nonlinear wave phenomena for a range of dispersive physical systems. Their stable multi-soliton solutions play an important role in the study of nonlinear waves [1]. Further studies have also been carried out to examine the effects on these solitons due to dissipation, inhomogeneity or non-uniformity present in nonlinear media [2, 3].

The term “soliton” is a sophisticated mathematical concept that derives its name from the word “solitary wave” which is a localized wave of translation that arises from the balance between nonlinear and dispersive effects [1]. In spite of the initial theoretical investigations, the concept of solitary wave could not gain wide recognition for a number of years in the midst of excitement created by the development of electromagnetic concepts in those times. Korteweg and de Vries (1895) developed a mathematical model for the shallow water problem and demonstrated the possibility of solitary wave generation [4]. Next, the study of solitary waves really took off in the mid-1960s when Zabusky and Kruskal discovered the remarkably stable particle-like behaviour of solitary waves [5]. They reported numerical experiments where

*Corresponding Author: Email: hejingsong@nbu.edu.cn, Tel: 86-574-87600739, Fax: 86-574-87600744.

solitary waves, described by the KdV equation, passed through each other unchanged in speed or shape, which led them to coin the word “soliton” to suggest such a unique property. In a follow-up study Zakharov and Shabat generalized the inverse scattering method in 1972 and also solved the nonlinear Schrödinger equation, demonstrating both its integrability and the existence of soliton solutions [6].

Following the above discoveries, solitary waves of all flavors advanced rapidly in many areas of science and technology. In nonlinear physics applications to many areas e.g. hydrodynamics, biophysics, atomic physics, nonlinear optics, etc., have been developed. As of now, more than a few hundreds of nonlinear evolution equations (NEEs) have been shown to admit solitons and some of these theoretical equations are also responsible for the experimental discovery of solitons [1, 7]. In general, nonlinear phenomena are often modelled by nonlinear evolution equations exhibiting a wide range of high complexities in terms of difference in linear and nonlinear effects. In the past four decades or so, the advent of high-speed computers, many advanced mathematical softwares and the development of a number of sophisticated and systematic analytical methods, which are well-supported by experiments have encouraged both theoreticians and experimentalists. Nonlinear science has experienced an explosive growth by the invention of several exciting and fascinating new concepts not just like solitons, but e.g. dispersion-managed solitons, rogue waves, similaritons, supercontinuum generation, etc. [1]. Many of the completely integrable nonlinear partial differential equations (NPDEs) admit one of the most striking aspects of nonlinear phenomena, which describe soliton as a universal character and they are of great mathematical as well as physical interest. It is impossible to discuss all these manifestations exhaustively in this paper. We further restrict ourselves to the solitary wave manifestation in nonlinear optics. In the area of soliton research at the forefront, right now, is the study of optical solitons, where the highly sought-after goal is to use strong localized nonlinear optical pulses as the high-speed information-carrying bits in optical fibers.

Optical solitons are localized electromagnetic waves that propagate steadily in a nonlinear medium resulting from the robust balance between nonlinearity and linear broadening due to dispersion and diffraction. Existence of the optical soliton was first time found in 1973 when Hasegawa and Tappert demonstrated the propagation of a pulse through a nonlinear optical fiber described by the nonlinear Schrödinger equation [8]. They performed a number of computer simulations demonstrating that nonlinear pulse transmission in optical fibers would be stable. Subsequently, after the fabrication of low-loss fiber, Mollenauer et al. in 1980 successfully confirmed this theoretical prediction of soliton propagation in a laboratory experiment [7]. Since then, fiber solitons have emerged as a very promising potential candidate in long-haul fiber optic communication systems.

Further, in addition to several important developments in soliton theory, the concept of modulational instability (MI) has also been widely used in many nonlinear systems to explain why experiments involving white coherent light supercontinuum generation (SCG), admit a triangular spectrum which can be described by the analytical expressions for the spectra of Akhmediev breather solutions at the point of extreme compression [1]. In the case of the NLS equation, Peregrine already in [9] had identified the role of MI in the formation of patterns resembling high-amplitude freak waves or rogue wave (RW). RWs have recently been also reported in different areas of science. In particular, in photonic crystal fibre RWs are well-established in connection with SCG [10]. This actually has stimulated research for RWs in other physical systems and has paved the way for a number important applications, including the control of RWs by means of SCG [11, 12], as well as studies in e.g. superfluid Helium [13], Bose Einstein condensates [14], plasmas [15, 16], microwave [17], capillary phenomena [18],

telecommunication data streams [19], inhomogeneous media [20], water experiments [21], and so on. Recently, Kibler *et al.* [22] using a suitable experiment with optical fibres were able to generate femtosecond pulses with strong temporal and spatial localization and near-ideal temporal Peregrine soliton characteristics.

For the past couple of years, several nonlinear evolution equations were shown to exhibit the RW-type rational solutions [23–39]. From the above listed works, it is clear that one of the possible generating mechanisms [40] for the higher-order RW is the interaction of multiple breathers possessing identical and very particular frequency of the underlying equation. Though the theory of solitons and many mathematical methods have been well-used in connection with soliton theory for the past four decades or so, to the best of our knowledge, the dynamics of multi-rogue wave evolutions has not yet been systematically investigated in integrable nonlinear systems [41].

Very recently, considering the propagation of few-cycle optical pulses in cubic nonlinear media and by developing multiple scaling approach to the Maxwell-Bloch-Heisenberg equation up to the third-order in terms of expansion parameter, the complex mKdV equation was derived [42, 43]. Circularly polarized few-cycle optical solitons were found which are valid for long pulses. Thus, it is more than worthy to systematically investigate the existence of the few-cycle optical rogue waves for this model, and this is the main purpose of the present paper.

The organization of this paper is as follows. In Section 2, based on the parameterized Darboux transformation (DT) of the mKdV equation, the general formation of the solution is given. In Section 3, we construct the higher-order rogue waves from a periodic seed with constant amplitude and analyze their structures in detail by choosing suitable system parameters. We provide detailed discussion about the obtained results in Sections 4 and 5.

2. THE DARBOUX TRANSFORMATION

For our analysis, we begin with coupled complex mKdV equations of the form of

$$q_t + q_{xxx} - 6qrq_x = 0, \quad (1)$$

$$r_t + r_{xxx} - 6rqr_x = 0. \quad (2)$$

Under a reduction condition $q = -r^*$, the above coupled equations reduce to the complex mKdV

$$q_t + q_{xxx} + 6|q|^2 q_x = 0. \quad (3)$$

The complex mKdV equation is one of the well-known and completely integrable equations in soliton theory, which possesses all the basic characters of integrable models. From a physical point of view, the above equation has been derived for, e.g. the dynamical evolution of nonlinear lattices, plasma physics, fluid dynamics, ultra-short pulses in nonlinear optics, nonlinear transmission lines and so on [41]. The Lax pair corresponding to the coupled mKdV equations is given by [41], i.e.

$$\psi_x = M\psi, \quad (4)$$

$$\psi_t = (V_3\lambda^3 + V_2\lambda^2 + V_1\lambda + V_0)\psi = N\psi, \quad (5)$$

with

$$\psi = \begin{pmatrix} \phi_1 \\ \phi_2 \end{pmatrix}, M = \begin{pmatrix} -i\lambda & q \\ r & i\lambda \end{pmatrix}, V_3 = \begin{pmatrix} -4i & 0 \\ 0 & 4i \end{pmatrix},$$

$$V_2 = \begin{pmatrix} 0 & 4q \\ 4\gamma & 0 \end{pmatrix}, V_1 = \begin{pmatrix} -2iqr & 2iq_x \\ -2ir_x & 2iqr \end{pmatrix},$$

$$V_0 = \begin{pmatrix} -qr_x + q_x r & -q_{xx} + 2q^2 r \\ -r_{xx} + 2qr^2 & qr_x - q_x r \end{pmatrix}.$$

Here, λ is an arbitrary complex spectral parameter or also called eigenvalue, and ψ is the eigenfunction corresponding to λ of the complex mKdV equation. From the compatibility condition $M_t - N_x + [M, N] = 0$, one can easily obtain the coupled equations (1) and (2). Furthermore, set T be a gauge transformation by

$$\psi^{[1]} = T\psi, q \rightarrow q^{[1]}, r \rightarrow r^{[1]}, \quad (6)$$

and

$$\psi_x^{[1]} = M^{[1]}\psi^{[1]}, \quad M^{[1]} = (T_x + TM)T^{-1}, \quad (7)$$

$$\psi_t^{[1]} = N^{[1]}\psi^{[1]}, \quad N^{[1]} = (T_t + TN)T^{-1}. \quad (8)$$

Here, $M^{[1]} = M(\rightarrow q^{[1]}, r \rightarrow r^{[1]})$, $N^{[1]} = N(q \rightarrow q^{[1]}, r \rightarrow r^{[1]})$. By cross-differentiating (7) and (8), we obtain

$$M_t^{[1]} - N_x^{[1]} + [M^{[1]}, N^{[1]}] = T(M_t - N_x + [M, N])T^{-1}. \quad (9)$$

This implies that, in order to prove that the mKdV equation is invariant under the gauge transformation (6), it is important to look for determine the T such that $M^{[1]}$, $N^{[1]}$ have the same forms as M , N . Meanwhile, the seed solutions (q, r) in spectral matrixes M , N are mapped into the new solutions $(q^{[1]}, r^{[1]})$ in terms of transformed spectral matrixes $M^{[1]}$, $N^{[1]}$.

Recently, using the generalized Darboux transformation, n th-order rogue wave solutions for the complex mKdV equation have been proposed in e.g. [38]. However, in our work, we shall systematically analyze the evolution of the different patterns of higher-order rogue waves by suitably choosing the parameters in the rational solutions. In addition, it is worth to note that the obtained results are in agreement with our recently published developments about the method of generating higher-order rogue waves [39, 40].

2.1 One-fold Darboux Transformation

From the knowledge of the known form of the DT for the nonlinear Schrödinger equation [44–49], we assume that a trial Darboux matrix T in eq. (6) has the following form

$$T = T(\lambda) = \begin{pmatrix} a_1 & b_1 \\ c_1 & d_1 \end{pmatrix} \lambda + \begin{pmatrix} a_0 & b_0 \\ c_0 & d_0 \end{pmatrix}, \quad (10)$$

where $a_0, b_0, c_0, d_0, a_1, b_1, c_1, d_1$ are functions of x and t . From

$$T_x + TM = M^{[1]}T, \quad (11)$$

by comparing the coefficients of λ^j , $j = 2, 1, 0$, it yields

$$\begin{aligned} \lambda^2 : & b_1 = 0, \quad c_1 = 0, \\ \lambda^1 : & a_{1x} = 0, \quad -2ib_0 + q_1 d_1 - qa_1 = 0, \\ & d_{1x} = 0, \quad -rd_1 + r_1 a_1 + 2ic_0 = 0, \\ \lambda^0 : & q_1 c_0 - a_{0x} - rb_0 = 0, \quad -b_{0x} + q_1 d_0 - qa_0 = 0, \\ & r_1 a_0 - c_{0x} - rd_0 = 0, \quad r_1 b_0 - d_{0x} - qc_0 = 0. \end{aligned} \quad (12)$$

From the coefficients of λ^1 , we conclude that a_1 and d_1 are functions of t only. Similarly, from

$$T_t + TN = N^{[1]}T, \quad (13)$$

and by comparing the coefficients of λ^j , $j = 3, 2, 1, 0$, we obtain the following set of equations

$$\begin{aligned}
\lambda^3 : & q_1 d_1 - q a_1 - 2i b_0 = 0, \quad r_1 a_1 - r d_1 + 2i c_0 = 0, \\
\lambda^2 : & -q_1 r_1 a_1 i + 2q_1 c_0 + a_1 q r i - 2r b_0 = 0, \quad -a_1 q_x i + 2q_1 d_0 - 2q a_0 + q_{1x} d_1 i = 0, \\
& 2r_1 a_0 - r_{1x} a_1 i - 2r d_0 + d_1 r_x i = 0, \quad q_1 r_1 d_1 i + 2r_1 b_0 - 2q c_0 - d_1 q r i = 0, \\
\lambda^1 : & -a_{1t} + r_1 q_{1x} a_1 + a_1 q r_x - a_1 r q_x + 2i q_{1x} c_0 + 2i b_0 r_x - 2i q_1 r_1 a_0 + 2i a_0 q r - q_1 r_{1x} a_1 = 0, \\
& -2i q_1 r_1 b_0 - 2i b_0 q r + a_1 q_{xx} + 2i q_{1x} d_0 - 2i a_0 q_x - 2a_1 q^2 r - q_{1xx} d_1 + 2q_1^2 r_1 d_1 = 0, \\
& -r_{1xx} a_1 + 2i q_1 r_1 c_0 + 2q_1 r_1^2 a_1 + 2i q r c_0 - 2i a_0 r_{1x} + 2i d_0 r_x - 2d_1 q r^2 + d_1 r_{xx} = 0, \\
& -d_{1t} - 2i c_0 q_x + 2i q_1 r_1 d_0 - r_1 q_{1x} d_1 - 2i r_{1x} b_0 - d_1 q r_x + d_1 r q_x - 2i d_0 q r + q_1 r_{1x} d_1 = 0, \\
\lambda^0 : & -q_{1xx} c_0 + b_0 r_{xx} + 2q_1^2 r_1 c_0 + a_0 q r_x - 2b_0 q r^2 + r_1 q_{1x} a_0 - q_1 r_{1x} a_0 - a_0 r q_x - a_{0t} = 0, \\
& a_0 q_{xx} - b_0 q r_x - b_0 q_1 r_{1x} - 2a_0 q^2 r + r_1 q_{1x} b_0 + 2q_1^2 r_1 d_0 + b_0 r q_x - q_{1xx} d_0 - b_{0t} = 0, \\
& -r_{1xx} a_0 + d_0 r_{xx} - r_1 q_{1x} c_0 + 2q_1 r_1^2 a_0 + q_1 r_{1x} c_0 - c_0 r q_x + c_0 q r_x - 2d_0 q r^2 - c_{0t} = 0, \\
& -r_1 q_{1x} d_0 + q_1 r_{1x} d_0 - r_{1xx} b_0 + 2q_1 r_1^2 b_0 + c_0 q_{xx} + d_0 r q_x - d_0 q r_x - 2c_0 q^2 r - d_{0t} = 0. \quad (14)
\end{aligned}$$

By making use of eq. (12) and eq. (14), one may obtain $a_{1x} = 0$, $d_{1x} = 0$, $a_{1t} = 0$, $d_{1t} = 0$, which implies that a_1 and d_1 are two constants.

In order to obtain the non-trivial solutions of the complex mKdV equation, we provide the Darboux transformation under the condition $a_1 = 1$, $d_1 = 1$. Without loss of generality, and based on eqs. (12) and (14), we observe that the Darboux matrix T admits the following form

$$T = T(\lambda) = \begin{pmatrix} 1 & 0 \\ 0 & 1 \end{pmatrix} \lambda + \begin{pmatrix} a_0 & b_0 \\ c_0 & d_0 \end{pmatrix}. \quad (15)$$

Here, a_0 , b_0 , c_0 , d_0 are functions of x and t , which could be expressed by two eigenfunctions corresponding to λ_1 and λ_2 . To begin with, we introduce $2n$ eigenfunctions ψ_j and $2n$ associated distinct eigenvalues λ_j as follows

$$\psi_j = \begin{pmatrix} \phi_{j1} \\ \phi_{j2} \end{pmatrix}, \quad j = 1, 2, \dots, 2n, \quad \phi_{j1} = \phi_1(x, t, \lambda_j), \quad \phi_{j2} = \phi_2(x, t, \lambda_j). \quad (16)$$

Note $\phi_1(x, t, \lambda)$ and $\phi_2(x, t, \lambda)$ are two components of eigenfunction ψ associated with λ in eqs. (4) and (5). Here, it is worthwhile to note that since the eigenfunction

$$\psi_j = \begin{pmatrix} \phi_{j1} \\ \phi_{j2} \end{pmatrix}$$

is the solution of the eigenvalue equations (4) and (5) corresponding to λ_j , and the eigenfunction

$$\psi'_j = \begin{pmatrix} -\phi_{j2}^* \\ \phi_{j1}^* \end{pmatrix}$$

is also the solution of eqs. (4) and (5) corresponding to λ_j^* , where $*$ denotes the complex conjugate.

We assume from now on that even number eigenfunctions and eigenvalues are given by odd ones as the following rule ($j = 1, 2, \dots, n$):

$$\lambda_{2j} = \lambda_{2j-1}^*, \quad \phi_{2j,1} = -\phi_{2j-1,2}^*(\lambda_{2j-1}), \quad \phi_{2j,2} = \phi_{2j-1,1}^*(\lambda_{2j-1}). \quad (17)$$

For convenience and simplicity of our mathematical manipulations, we propose the following theorems:

Theorem 1. *The elements of a one-fold Darboux matrix are presented with the eigenfunction ψ_1 corresponding to the eigenvalue λ_1 as follows*

$$\begin{aligned} a_0 &= -\frac{1}{\Delta_2} \begin{vmatrix} \lambda_1 \phi_{11} & \phi_{12} \\ \lambda_2 \phi_{21} & \phi_{22} \end{vmatrix}, \quad b_0 = \frac{1}{\Delta_2} \begin{vmatrix} \lambda_1 \phi_{11} & \phi_{11} \\ \lambda_2 \phi_{21} & \phi_{21} \end{vmatrix}, \\ c_0 &= \frac{1}{\Delta_2} \begin{vmatrix} \phi_{12} & \lambda_1 \phi_{12} \\ \phi_{22} & \lambda_2 \phi_{22} \end{vmatrix}, \quad d_0 = -\frac{1}{\Delta_2} \begin{vmatrix} \phi_{11} & \lambda_1 \phi_{12} \\ \phi_{21} & \lambda_2 \phi_{22} \end{vmatrix}, \end{aligned} \quad (18)$$

$$\Leftrightarrow T_1(\lambda; \lambda_1) = \begin{pmatrix} \lambda - \frac{1}{\Delta_2} \begin{vmatrix} \lambda_1 \phi_{11} & \phi_{12} \\ \lambda_2 \phi_{21} & \phi_{22} \end{vmatrix} & \frac{1}{\Delta_2} \begin{vmatrix} \lambda_1 \phi_{11} & \phi_{11} \\ \lambda_2 \phi_{21} & \phi_{21} \end{vmatrix} \\ \frac{1}{\Delta_2} \begin{vmatrix} \phi_{12} & \lambda_1 \phi_{12} \\ \phi_{22} & \lambda_2 \phi_{22} \end{vmatrix} & \lambda - \frac{1}{\Delta_2} \begin{vmatrix} \phi_{11} & \lambda_1 \phi_{12} \\ \phi_{21} & \lambda_2 \phi_{22} \end{vmatrix} \end{pmatrix}, \quad (19)$$

with $\Delta_2 = \begin{vmatrix} \phi_{11} & \phi_{12} \\ \phi_{21} & \phi_{22} \end{vmatrix}$, and then the new solutions $q^{[1]}$ and $r^{[1]}$ are given by

$$q^{[1]} = q + 2i \frac{1}{\Delta_2} \begin{vmatrix} \lambda_1 \phi_{11} & \phi_{11} \\ \lambda_2 \phi_{21} & \phi_{21} \end{vmatrix}, \quad r^{[1]} = r - 2i \frac{1}{\Delta_2} \begin{vmatrix} \phi_{12} & \lambda_1 \phi_{12} \\ \phi_{22} & \lambda_2 \phi_{22} \end{vmatrix}, \quad (20)$$

and the new eigenfunction $\psi_j^{[1]}$ corresponding to λ_j is

$$\psi_j^{[1]} = T_1(\lambda; \lambda_1)|_{\lambda=\lambda_j} \psi_j. \quad (21)$$

Proof. Note that $b_1 = c_1 = 0$, $a_{1x} = 0$ and $d_{1x} = 0$ is derived from the functional form of x , then $a_{1t} = 0$ and $d_{1t} = 0$ is derived from the functional form of t . So, a_1 and d_1 are arbitrary constants, and hence, we let $a_1 = d_1 = 1$ for simplicity for later calculations. By transformation defined by eq. (12) and eq. (14), new solutions are given by

$$q_1 = q + 2ib_0, r_1 = r - 2ic_0. \quad (22)$$

By making use of the general property of the DT, i.e., $T_1(\lambda; \lambda_j)|_{\lambda=\lambda_1} \psi_j = 0$, $j = 1, 2$, after some manipulations, eq. (18) is obtained. Next, substituting (a_0, b_0, c_0, d_0) given in eq. (18) into eq. (22), the new solutions are given as in eq. (20). Furthermore, by using the explicit matrix representation eq. (19) of T_1 , then $\psi_j^{[1]}$ ($j \geq 3$) is given by $\psi_j^{[1]} = T_1(\lambda; \lambda_1)|_{\lambda=\lambda_j} \psi_j$. \square

It is trivial to confirm $q^{[1]} = -(r^{[1]})^*$ by using the special choice on ψ_2 and λ_2 in eq. (17). This means $q^{[1]}$ generates a new solution of the complex mKdV from a seed solution q . Note that $\psi_j^{[1]} = 0$ for $j = 1, 2$.

2.2 n-fold Darboux transformation

By n -times iteration of the one-fold DT T_1 , we obtain n -fold DT T_n of the complex mKdV equation with the special choice on λ_{2j} and ψ_{2j} in eq. (17). To save space, we omit the tedious calculation of T_n and its determinant representation. Under the above conditions, the reduction condition $q^{[n]} = -(r^{[n]})^*$ is preserved by T_n , so we just give $q^{[n]}$ in the following theorem.

Theorem 2. *Under the choice of eq. (17), the n -fold DT T_n generates a new solution of the complex mKdV equation from a seed solution q as*

$$q^{[n]} = q - 2i \frac{N_{2n}}{D_{2n}}, \quad (23)$$

where

$$N_{2n} = \begin{vmatrix} \phi_{11} & \phi_{12} & \lambda_1 \phi_{11} & \lambda_1 \phi_{12} & \dots & \lambda_1^{n-1} \phi_{11} & \lambda_1^n \phi_{11} \\ \phi_{21} & \phi_{22} & \lambda_2 \phi_{21} & \lambda_2 \phi_{22} & \dots & \lambda_2^{n-1} \phi_{21} & \lambda_2^n \phi_{21} \\ \phi_{31} & \phi_{32} & \lambda_3 \phi_{31} & \lambda_3 \phi_{32} & \dots & \lambda_3^{n-1} \phi_{31} & \lambda_3^n \phi_{31} \\ \phi_{41} & \phi_{42} & \lambda_4 \phi_{41} & \lambda_4 \phi_{42} & \dots & \lambda_4^{n-1} \phi_{41} & \lambda_4^n \phi_{41} \\ \vdots & \vdots & \vdots & \vdots & \vdots & \vdots & \vdots \\ \phi_{2n1} & \phi_{2n2} & \lambda_{2n} \phi_{2n1} & \lambda_{2n} \phi_{2n2} & \dots & \lambda_{2n}^{n-1} \phi_{2n1} & \lambda_{2n}^n \phi_{2n1} \end{vmatrix},$$

$$D_{2n} = \begin{vmatrix} \phi_{11} & \phi_{12} & \lambda_1 \phi_{11} & \lambda_1 \phi_{12} & \dots & \lambda_1^{n-1} \phi_{11} & \lambda_1^{n-1} \phi_{12} \\ \phi_{21} & \phi_{22} & \lambda_2 \phi_{21} & \lambda_2 \phi_{22} & \dots & \lambda_2^{n-1} \phi_{21} & \lambda_2^{n-1} \phi_{22} \\ \phi_{31} & \phi_{32} & \lambda_3 \phi_{31} & \lambda_3 \phi_{32} & \dots & \lambda_3^{n-1} \phi_{31} & \lambda_3^{n-1} \phi_{32} \\ \phi_{41} & \phi_{42} & \lambda_4 \phi_{41} & \lambda_4 \phi_{42} & \dots & \lambda_4^{n-1} \phi_{41} & \lambda_4^{n-1} \phi_{42} \\ \vdots & \vdots & \vdots & \vdots & \vdots & \vdots & \vdots \\ \phi_{2n1} & \phi_{2n2} & \lambda_{2n} \phi_{2n1} & \lambda_{2n} \phi_{2n2} & \dots & \lambda_{2n}^{n-1} \phi_{2n1} & \lambda_{2n}^{n-1} \phi_{2n2} \end{vmatrix}.$$

By making use of Theorem 2 with a suitable seed solution, we can generate the multi-solitons, multi-breathers, and multi-rogue waves of the complex mKdV equation. As the multi-soliton and multi-breather solutions are well-known and completely explored for the complex mKdV equation, next, we shall concentrate mainly on the systematic construction of the higher-order rogue waves from the double degeneration [40] of the DT. Though the construction of higher-order rogue wave solutions is quite cumbersome, one can still validate the correctness of these solutions with the help of modern computer tools such as a simple symbolic calculation or equivalent, and also by a direct numerical computation.

3. HIGHER-ORDER ROGUE WAVES

In this section, starting with a non-zero seed $q = ce^{i\rho}$, $\rho = ax + bt$, $b = a^3 - 6ac^2$, $a, b, c \in \mathbb{R}$, we shall present higher-order rogue waves of the complex mKdV equation. If $a = 0$, $q = c$ a constant, which is just a seed solution to generate soliton. So, in this paper, we choose $a \neq 0$. By using the principle of superposition of the linear differential equations, then, the new eigenfunctions corresponding to λ_j can be provided by

$$\psi_j = \begin{pmatrix} d_1 ce^{i[(\frac{1}{2}a+c_1)x+(\frac{1}{2}b+2c_1c_2)t]} + d_2 i(\frac{1}{2}a + \lambda_j + c_1) e^{i[(-\frac{1}{2}a+c_1)x+(-\frac{1}{2}b+2c_1c_2)t]} \\ d_1 i(\frac{1}{2}a + \lambda_j + c_1) e^{-i[(-\frac{1}{2}a+c_1)x+(-\frac{1}{2}b+2c_1c_2)t]} + d_2 ce^{-i[(\frac{1}{2}a+c_1)x+(\frac{1}{2}b+2c_1c_2)t]} \end{pmatrix} \quad (24)$$

with

$$d_1 = e^{ic_1(s_0+s_1\varepsilon+s_2\varepsilon^2+\dots+s_{n-1}\varepsilon^{n-1})}, \quad d_2 = e^{-ic_1(s_0+s_1\varepsilon+s_2\varepsilon^2+\dots+s_{n-1}\varepsilon^{n-1})},$$

$$c_1 = \frac{1}{2}\sqrt{a^2 + 4c^2 + 4\lambda_j a + 4\lambda_j^2}, \quad c_2 = 2\lambda_j^2 - c^2 + \frac{1}{2}a^2 - \lambda_j a. \quad (25)$$

Here, $s_i \in \mathcal{C}$ ($i = 0, 1, 2, \dots, n-1$), $a, b, c \in \mathbb{R}$ are the arbitrary constants, ε is an infinitesimal parameter.

We are now in a position to consider the double degeneration of $q^{[n]}$ to obtain higher-order rogue wave as in our earlier investigations [40]. It is trivial to check that $\psi_j(\lambda_0) = 0$ in eq. (24), which means that these eigenfunctions are degenerate at $\lambda_0 = ic - \frac{a}{2}$. Setting $\lambda_{2j-1} \rightarrow \lambda_0$ and substituting ψ_{2j-1} ($j = 1, 2, \dots, n$) defined by eq. (24) back into eq. (23), the double degeneration, i.e. eigenvalue and eigenfunction degeneration, occurs in $q^{[n]}$. Next, $q^{[n]}$ now becomes an indeterminate form $\frac{0}{0}$. Set $\lambda_{2j-1} = \lambda_0 + \epsilon$ and set ψ_{2j-1} be given by eq. (24), we obtain n -th order rogue wave solutions by higher-order Taylor expansion of $q^{[n]}$ with respect to ϵ .

Theorem 3. An n -fold degenerate DT with a given eigenvalue λ_0 is realized in the degenerate limit $\lambda_j \rightarrow \lambda_0$ of T_n . This degenerate n -fold DT yields a new solution $q^{[n]}$ of the mKdV equation starting with the seed solution q , where

$$q^{[n]}(x, t; \lambda_0) = q - 2i \frac{N'_{2n}}{D'_{2n}}, \quad (26)$$

with

$$D'_{2n} = \left(\frac{\partial^{n_i}}{\partial \varepsilon^{n_i}} \Big|_{\varepsilon=0} (D_{2n})_{ij}(\lambda_0 + \varepsilon) \right)_{2n \times 2n},$$

$$N'_{2n} = \left(\frac{\partial^{n_i}}{\partial \varepsilon^{n_i}} \Big|_{\varepsilon=0} (N_{2n})_{ij}(\lambda_0 + \varepsilon) \right)_{2n \times 2n}.$$

Here, $n_i = [\frac{i+1}{2}]$, $[i]$ denotes the floor function of i .

In the following, to avoid the tedious mathematical steps we encountered, we only present the expressions of the 1st, 2nd and 3rd order rogue waves by using Theorem 3. In each case, the solution $q^{[n]}$ describes the envelope of the rogue wave, and its square modulus contains information such as e.g. wave evolution above water surface, or the intensity of few-cycle optical wave, etc.

Firstly, we set $n = 1$, D_2 and N_2 take the form of 2×2 determinants. By using the 1st-order Taylor expansion with respect to ε in terms of elements of D_2 and N_2 through $\lambda_1 = \lambda_0 + \varepsilon$, we determined N'_2 and D'_2 by equating the coefficient of $\sqrt{\varepsilon}$, and then obtained the explicit expression for the 1st-order rogue wave as

$$q^{[1]} = -ce^{ia(x+t(a^2-6c^2))} \frac{A + 48ic^2ta - 3}{A + 1}, \quad (27)$$

with $A = 24ta^2c^2x + 24ta^2c^2s_0 + 36t^2a^4c^2 - 48c^4tx - 48c^4ts_0 + 8c^2xs_0 + 144c^6t^2 + 4c^2x^2 + 4c^2s_0^2$. Its evolution is presented in Figure 1 (left) with the condition $d_1 = d_2 = 1$ and the Taylor expansion at $\lambda_0 = ic - \frac{a}{2} + \varepsilon$, in order to compare this with higher-order rogue waves. It is trivial to find that $|q^{[1]}|^2 = c^2$ when $x \rightarrow \infty$ and $t \rightarrow \infty$. This means that the asymptotic plane of $|q^{[1]}|^2$ has the height c^2 . Particularly, let $a = 0$ and $s_0 = 0$, $|q^{[1]}|^2$ is a soliton propagating along a line $x = 6c^2t$ with a non-vanishing boundary. Set $c = -1$, $a = \sqrt{6}$, $s_0 = 0$ and $t \rightarrow t/2$, then $q^{[1]}$ gives $u[2]$ of ref. [38].

When $n = 2$, we construct the 2nd-order rogue waves under the assumption $d_1 = e^{ic_1(s_0+s_1\varepsilon)}$, $d_2 = e^{-ic_1(s_0+s_1\varepsilon)}$, $s_0 = 0$ from Theorem 3. An explicit form of $q^{[2]}$ is constructed as

$$q^{[2]} = ce^{ia(x+t(a^2-6c^2))} \frac{B}{C}. \quad (28)$$

Here, B and C are two degree 6 polynomials in x and t , which are given in appendix A. From Figure 1 (right), one finds that under the assumption $d_1 = 1, d_2 = 1$, or equivalently $s_0 = s_1 = 0$, the second-order rational solution admits a single high maximum at the origin. By suitably adjusting the parameter a one could control the decaying rate of the profile in the (x, t) -plane. This is a fundamental pattern. Furthermore, as is shown in Figure 6, when taking $d_1 \neq 1$ and $d_2 \neq 1$, the large peak of the 2nd rogue wave is completely separated and forms a set of three first-order rational solution for sufficiently large s_1 meanwhile $s_0 = 0$, and actually forms an equilateral triangle.

When $n = 3$, and set $d_1 = e^{ic_1(s_0+s_1\varepsilon+s_2\varepsilon^2)}$ and $d_2 = e^{-ic_1(s_0+s_1\varepsilon+s_2\varepsilon^2)}$, then Theorem 3 yields an explicit formula of the 3rd rogue wave with parameters a, c, s_0, s_1, s_2 . Set $a = 1.5, c = 1, s_0 =$

$s_1 = s_2 = 0$, we have

$$q^{[3]} = \frac{L_1}{L_2} e^{i(\frac{3}{2}x - \frac{45}{8}t)}. \quad (29)$$

Here, L_1 and L_2 are two degree 12 polynomials in x and t , which are given in appendix B. This is the fundamental pattern of the 3rd-order rogue wave, which is plotted in Figure 2(left) with a different value of a .

In general, Theorem 3 provides an efficient tool to produce analytical forms of higher-order rogue waves of the complex mKdV equation. Actually, we have also constructed the analytical formulas for 4th, 5th and 6th -order rogue waves. However, because of their long expressions describing these solutions, we do not present them here but would provide upon request. The validity of all these higher-order rogue waves has been verified by symbolic computation. According to the explicit formulae of the n th-order rogue waves under fundamental patterns, we find that their maximum amplitude is $(2n+1)^2 c^2$ ($n = 1, 2, 3, 4, 5, 6$) by setting $x = 0$ and $t = 0$ in $|q^{[n]}|^2$, and the height of the asymptotic plane is c^2 , which is the same as that of the rogue wave of the NLS equation. This fact can be easily verified through Figs.(1-3). All figures in this paper are plotted based on these explicit analytical formulas of the solutions. Once the explicit analytical higher-order rogue waves are known, our next aim is to generate and understand underlying the dynamics of the obtained different patterns by suitably selecting the value of s_i .

4. RESULTS AND DISCUSSION

The above discussion is a clear manifestation of the evolution of the higher-order rogue waves from the Taylor expansion of the degenerate breather solutions. A brief discussion about the generating mechanism of higher-order rogue waves from the nonlinear evolution equation has already been reported by [40]. For our purpose now, we customize our discussion only up to 6th-order rogue waves, since higher-order rogue waves are difficult to construct owing to the extreme complexity and tedious mathematical calculations. It is quite obvious from our numerical analysis that the choice of parameters such as d_1 and d_2 actually do generate three different basic patterns of rogue wave solutions. Let us discuss these patterns now.

Fundamental patterns: When, e.g. $d_1 = d_2 = 1$, or equivalently $s_i = 0$ ($i = 0, 1, 2, \dots, n-1$) in $q^{[n]}$, the rational solutions of any order n have a similar structure. In addition, there are $\frac{n(n+1)}{2} - 1$ local maxima on each side of the line at $t = 0$. Starting from ∞ , before the central optimum high amplitude, there is a sequence of peaks with gradual increase in height. Here, one can observe that the number of first peaks is n , then there is a row of $n - 1$ symmetric peaks with respect to time t as shown in Figs. (1-3) for 6 rogue waves.

There are only two parameters a and c in the explicit forms of the rogue waves under fundamental patterns. It is a challenge problem to illustrate analytically the role of a and c in the control of the profile for the higher-order RWs due to the extreme complexity of the explicit forms of the n th-order RWs ($n \geq 2$). So, we only study this problem for the first-order RW $|q^{[1]}|^2$. To this end, we introduce a method, i.e., the contour line method, to analyze the contour profile of the red bright spots in the density plot of Fig. 4, which intuitively shows the localization characters such as length and width of the RW. On the background plane with height c^2 , a contour line of $|q^{[1]}|^2$ with $c = 1$ is a hyperbola

$$x^2 - 12tx + 6ta^2x + 36t^2 - 72t^2a^2 + 9t^2a^4 - \frac{1}{4} = 0, \quad (30)$$

which has two asymptotes

$$l_1 : x = (6 - 3a^2 - 6a)t, \quad l_2 : x = (6 - 3a^2 + 6a)t, \quad (31)$$

and two non-orthogonal axes:

$$\text{major axis : } t = 0, \quad \text{imaginary axis}(l_3) : x = (6 - 3a^2)t. \quad (32)$$

There are two fixed vertices: $P_1 = (0, 0.50)$, $P_2 = (0, -0.5)$ on (t, x) plane of all value of a . Here, l_3 is also a median of one triangle composed of above two asymptotes and a parallel line of x -axis except $t = 0$. We combine the density plots and the above three lines in Fig.4 with different values of a . At height $c^2 + 1$, a contour line of $|q^{[1]}|^2$ with $c = 1$ is given by a quartic polynomial

$$x^4 + (12a^2 - 24)tx^3 + \left(\frac{5}{2} + (216 - 144a^2 + 54a^4)t^2\right)x^2 + ((-864 + 432a^2 - 216a^4 + 108a^6)t^3 + (15a^2 - 30)t)x + (1296 + 648a^4 + 81a^8)t^4 + (90 - 144a^2 + \left(\frac{45}{2}\right)a^4)t^2 - \frac{7}{16} = 0, \quad (33)$$

which has two end points $P_3 = (-\frac{\sqrt{7}}{12a}, \frac{(-2+a^2)\sqrt{7}}{4a})$ and $P_4 = (\frac{\sqrt{7}}{12a}, -\frac{(-2+a^2)\sqrt{7}}{4a})$ along t -direction.

Moreover, there are two fixed points expressed by $P_5 = (0, \frac{\sqrt{-1-4c^2+4\sqrt{c^2(c^2+1)}}}{2c}|_{c=1}) = (0, 0.41)$, $P_6 = (0, -\frac{\sqrt{-1-4c^2+4\sqrt{c^2(c^2+1)}}}{2c}|_{c=1}) = (0, -0.41)$ on (t, x) plane of all value of a . At height $\frac{c^2}{2}$, a contour line of $|q^{[1]}|^2$ with $c = 1$ is also given by a quartic polynomial

$$x^4 + (12a^2 - 24)tx^3 + ((216 - 144a^2 + 54a^4)t^2 - \frac{7}{2})x^2 + ((-864 + 432a^2 - 216a^4 + 108a^6)t^3 + (-21a^2 + 42)t)x + (1296 + 648a^4 + 81a^8)t^4 + (-126 + 288a^2 - \frac{63}{2}a^4)t^2 + \frac{17}{16} = 0, \quad (34)$$

which is defined on interval $[-\frac{1}{12a}, \frac{1}{12a}]$ of t . For this contour line, there are four fixed points: $(0, 1.78)$, $(0, 0.58)$, $(0, -0.58)$, $(0, -1.78)$ on (t, x) plane of all value of a . Two centers of valleys of $|q^{[1]}|^2$ given by $P_7 = (0, \frac{\sqrt{3}}{2c})$, $P_8 = (0, -\frac{\sqrt{3}}{2c})$, which are independent with the value of a . Fig.5 are plotted for above contour lines with different values of $a = 1.5, 2, 2.5$.

Based on the above analytical results, we could define the length and width of the rogue wave, which are two crucial characters of a doubly localized wave-RW. Because the contour line of RW on the background plane is not a closed curve, so we can not define a length for RW on this plane. However, set d be a positive constant, the contour line at height $c^2 + d$ is closed. Here $c^2 + d < 9c^2$, or equivalently $d < \sqrt{8c^2}$ because the max amplitude of the first-order RW ($|q^{[1]}|^2$) is $9c^2$. Without loss of generality, and considering a recognizable height from the asymptotic plane, we set $d = 1$ as before. We can use the length of the area surrounded by the contour line at height $c^2 + 1$ as the length of the first-order RW. The length-direction is defined by l_3 , the width-direction is orthogonal to it. The reasons for this choice are : 1) l_3 passes through P_3 and P_4 ; 2) l_3 is parallel to the tangent line of hyperbola at two vertices; 3) l_3 is parallel to the tangent line of the contour line at P_5 and P_6 . Let k_3 be the slope of l_3 . So the length of the first-order RW is the distance of P_3 and P_4 , i.e.,

$$d_L = \frac{\sqrt{7}}{6a} \sqrt{1 + (k_3)^2} = \frac{\sqrt{7}}{6a} \sqrt{1 + (6 - 3a^2)^2}. \quad (35)$$

The width is defined as the projection of line segment P_7P_8 at width-direction, which is expressed by

$$d_W = \frac{\sqrt{3}}{\sqrt{1 + (k_3)^2}} = \frac{\sqrt{3}}{\sqrt{1 + (6 - 3a^2)^2}}. \quad (36)$$

d_L and d_W are plotted in figure 6 with fixed $c = 1$, which shows that the length is decreased with a when $a \in (0, \sqrt{2})$ and is increased with a when $a > \sqrt{2}$. However, the width has an opposite increasing or decreasing trend with respect to a . When $a = \sqrt{2}$, the profile of first-order RW is parallel to the t -axis, then the length reaches to its minimum, and the width reaches to its maximum. This is the first role of a in the control of the RW. Moreover, we know from k_3 that the increase of a results in the rotation of RW in the clockwise direction. This is the second role of a .

In above discussion for the role of a , we have set $c = 1$. If $c \neq 1$, it is a more interesting and complicated case, which can be studied as above by using contour line method. To save the space, we shall provide corresponding results without explanation, which can be done by a similar way as above. Under this case, two asymptotes of the contour line of first-order RW $|q^{[1]}|^2$ at height c^2

$$\text{major axis : } t = 0, \quad \text{imaginary axis}(\text{cl}_3) : x = (6c^2 - 3a^2)t. \quad (37)$$

In other word, slope is $k_{3c} = 6c^2 - 3a^2$. Two vertices of the hyperbola are $P_1 = (0, \frac{1}{2c})$ and $P_2 = (0, -\frac{1}{2c})$ on (t, x) plane. For contour line at height $c^2 + 1$, two end points are $P_3 = (-\frac{\sqrt{8c^2-1}}{12ac^2}, \frac{(-2c^2+a^2)\sqrt{8c^2-1}}{4ac^2})$ and $P_4 = (\frac{\sqrt{8c^2-1}}{12ac^2}, -\frac{(-2c^2+a^2)\sqrt{8c^2-1}}{4ac^2})$ along t direction. So the length of the first-order RW is

$$d_{cL} = \frac{\sqrt{8c^2-1}}{6c^2a} \sqrt{1 + 9(-2c^2 + a^2)^2}, \quad (38)$$

and the width of the first-order RW is

$$d_{cW} = \frac{\sqrt{3}}{c} \frac{1}{\sqrt{1 + 9(-2c^2 + a^2)^2}}, \quad (39)$$

which are plotted in Figure 7. These pictured show visually the role of a and c in the control of the first-order RW. For a given value of a , d_{cL} has two extreme points with respect to c . However, for a given value of c , d_{cL} has one extreme point with respect to a . The slope k_{3c} shows that the increasing of a and c results in the rotation of the first-order RW with different direction. Note that $a = \sqrt{2}c$ is a line of points for extreme value. Under this condition, the profile of first-order RW is parallel to the t -axis, and the minimum of the length is $\frac{\sqrt{4a^2-1}}{3a^3}$, the maximum of the width is $\frac{\sqrt{3}}{c}$.

Triangular patterns: The triangular structure can be obtained by choosing the first non-trivial coefficient $s_1 \gg 1$, while the rest of the values are assumed to be zero. It can be seen from Figs. (8-10) that the n -th order rational solutions have $\frac{n(n+1)}{2}$ peaks of equal height with a structure of equilateral triangular type having n peaks at each edge.

Ring patterns: One can observe the ring structure/pattern when $n \geq 3$ and the principle coefficient for n -th order rational solution when $s_{n-1} \gg 1$, while the remaining coefficients s_i are all zero. The rational solutions consist of the outer circular shell of $2n-1$ first-order rational solutions, while the center is an order $(n-2)$ rational solution of the fundamental patterns as portrayed in Figs. (11-12). The center order- $(n-2)$ rogue wave can be decomposed further into different lower-order patterns according to the $(n-2)$ -reduction rule of order by setting one of s_i ($i = 0, 1, 2, \dots, n-3$) to non-zero, which are plotted in Figs. (13-15). For example, the center order-4 rogue wave of the 6-th rogue wave has a fundamental pattern (Figure 12 (right)), a ring plus a fundamental pattern (Figure 14 (right)) or triangular pattern ((Figure 15 (right))) of 2nd-order rogue wave, a triangular pattern (Figure 15 (left)). We call these forms

as standard decomposition of the rogue wave. This structure is similar to the so-called “wave clusters” as reported in [50].

Another interesting fact worth mentioning here is that the profiles of higher-order rogue wave are actually a complicated combination of above three basic patterns: “fundamental” pattern, “ring” pattern and “triangular” pattern, which can provide further interesting patterns of the rogue waves. This can be achieved by suitably selecting the different values of s_i . In particular, one can generate multi-ring structures but these rings do not possess $2n-1$ peaks and also do not satisfy the rule of $(n-2)$ -reduction of order as mentioned earlier in the case of ring pattern formation. Thus, we call these formations as non-standard decomposition of the rogue waves. Figures (16-20) represent a few examples of this kind of special ring structures. One common feature, which we observed from these examples, is the appearance of at least two ring patterns with the same number of peaks. It should be noted that the center-most profile of Figure 18 (left) is a fundamental pattern of a 2nd-order rogue wave, which clearly shows that Figure 18 (left) is not a complete decomposition of the 6-th order rogue wave. On the other hand, Figure 18 (right) presents the complete decomposition. To arrive to a better understanding of the non-standard decomposition, we provide the distribution of peaks in Table 1. From Figure 19 (left), it can also be observed the occurrence of two ring patterns with a single inner peak, however, the inner ring consists of 5 triangular patterns. So, the distribution of peaks is $5 + 3 \times 5 + 1$.

In spite of having different structures, all types of rogue wave solutions possess certain commonality as follows: The total number of peaks admitted by n -th order solutions is $\frac{n(n+1)}{2}$ in terms of a complete decomposition pattern. These structures actually depend on the choice of the free parameters. Among all parameters, the principle coefficient s_{n-1} is accountable for the formation of a ring structure. The first non-trivial coefficient s_1 is responsible for the evolution of a triangular structure. Furthermore, to see difference between the RWs of the complex mKdV and the NLS clearly, we use the first-order RW ([40]) of the NLS, i.e.,

$$q_{NLS}^{[1]} = c^2 \frac{\tilde{A} - 32c^2((-x + 2at)^2 - 4c^2t^2) + 8}{\tilde{A}}, \quad \tilde{A} = (4c^2x^2 - 16c^2xta + 16t^2(c^4 + c^2a^2) + 1)^2. \quad (40)$$

to calculate the contour lines at heights c^2 and $c^2 + 1$, and to calculate the length, width by the same procedure we have used in complex mKdV. Here the NLS equations is in the form of

$$iq_t + q_{xx} + 2|q|^2q = 0. \quad (41)$$

Similar to the contour line method of the complex mKdV, we get the slope of the imaginary axis of the hyperbola formed by a contour line of the $|q_{NLS}^{[1]}|^2$ on background plane with a height $c^2: k_{3cNLS} = 2a$, and the length of the RW

$$d_{cLNLS} = \frac{1}{2c^2} \sqrt{(-1 + 8c^2)(1 + 4a^2)}, \quad (42)$$

and the width of the RW

$$d_{cWNLS} = \frac{\sqrt{3}}{c \sqrt{1 + 4a^2}}. \quad (43)$$

The dynamical evolution of the first-order RW $|q_{NLS}^{[1]}|^2$ of the NLS are plotted in Fig. 21, contour lines at heights c^2 and $c^2 + 1$ of the first-order RWs of the complex mKdV and the NLS are plotted in Fig. 22. These pictures and analytical formulae of length and width show that, for the first-order RWs of the complex mKdV and the NLS, they are very similar to each other apart from a remarkable tilt with respect to the axes and a remarkable shortening of length of them with same values of a and c . In other words, the inclusion of third-order dispersion and

time-delay correction is responsible for a strong rotation and a strong compression effects in the first-order RW of the complex mKdV equation. In particular, if $a = 0$, $|q_{NLS}^{[1]}|^2$ is still a RW, but $|q^{[1]}|^2$ of the complex mKdV is a soliton traveling along l_3 which is no longer doubly-localized in x and t directions.

In terms of applications, the investigation of the above investigated higher-order RW solutions will be useful to understand the generation of high-power waves and their possible splitting, etc. As we have discussed earlier, very recently, using the non-slowly varying envelope approximation (SVEA), the complex mKdV equation has been derived and the generation of few-cycle optical pulses have been reported [42, 43]. In addition, it has been pointed out that these type of few-cycle optical pulses require no phase matching (a main issue in nonlinear optics), which makes a strong contrast and provides an interesting aspect when compared with the longer pulses derived by using the SVEA method. From these recent studies it is also interesting to note that these type of few-cycle optical pulses are very similar to the generation of high-power and very short RW type ultra-short pulses. For example, in nonlinear photonic crystal fibre, the above waves may be connected to the generation of few-cycle optical pulses which will be useful to realize the so-called supercontinuum generation. This type of white light continuum coherence source will find a range of applications in optical coherence tomography, optical meteorology, wavelength division multiplexing, fluorescence microscopy, flow cytometry, atmospheric sensing, etc. [1, 42, 43].

5. CONCLUSIONS

In this paper, we applied the DT to construct the higher-order RW-type rational solutions as well as the evolution of rogue waves for the complex mKdV equation. Based on detailed numerical and analytical investigations, we classified the higher-order RWs with respect to their intrinsic structure. We use the contour line method, for the first time to the best of our knowledge, to define the length and width of the first-order RW, and then provide their analytical formulae related to two parameters a and c . We illustrate clearly, by analytical formulas and figures, that the differences between the first-order RWs of the mKdV and the NLS are mainly due to strong rotation as well as strong compression effects. Furthermore, we observed that there are three principle types, namely, fundamental pattern, ring pattern, and triangular pattern. The composition of these three principle patterns is mainly because of higher-order rogue waves. We also provided several further new patterns of the higher-order RWs of this model. The ring patterns obtained in this paper are similar to the “atom” structure reported in [50]. This explains the generalization and evolution of higher-order RWs in terms of the solution. On the other hand, by changing the free parameters in the DT, we have also constructed more complicated (and interesting) structures. We deduced from our stimulated examples in Figs. 16-20 that the non-standard decomposition deserves further studies because there are presently unknown rules of the decomposition. Applying our construction of RW solutions to different completely integrable nonlinear evolution equations, it is interesting to investigate some analogues between the evolution and decomposition of higher-order RWs of these different integrable equations. It is essential to find further conserved quantities for the kind of solutions. These studies may help us for better understanding of the occurrence of deep ocean waves with large amplitude as well as the generation of few-cycle optical pulses emitted by high-power lasers which are used for the recently invented supercontinuum generation sources, etc.

If we compare our results with the work in [38] on the rogue wave solutions of the complex mKdV, our results have following advantages and developments:

- Our method is considerably simpler as well as more systematic. From Theorem 3, one can directly obtain the higher-order RWs without calculating eigenfunctions $\psi_1^{[i]}$ and $\phi_1^{[i]}$ ($i = 0, 1, 2, 3$) as in [38].
- We applied the contour line method to find the analytical description of the length and width of the first-order RW of the complex mKdV and the NLS equation. We illustrated clearly, using suitable analytical formulae and figures, that the differences between the first-order RWs of the mKdV and the NLS are due to a strong rotation and a strong compression effects. Note that, setting $a = 0$, $|q^{[1]}|^2$ reduces to a soliton on a background plane at height c^2 , but $|q_{NLS}^{[1]}|^2$ can not.
- We proposed and proved a convenient way to control the patterns and evolutions of the rogue wave by standard and non-standard decomposition with suitable choices of s_i .
- We generated interesting patterns for 4th, 5th and 6th rogue waves.

With respect to the future research in this exciting area, we shall apply the contour line method to the first-order RW of the different NLS type equations. For the higher-order rogue waves, because the degree of polynomials in its explicit form is more than 4, it is not easy to get the analytical expressions of the asymptotes for its contour lines in general. Thus, how to get the analytical results on their length and width is an interesting, difficult and important problem, which deserves further study.

Acknowledgments

This work is supported by the NSF of China under Grant No.11271210 and the K. C. Wong Magna Fund in Ningbo University. J.S. He thanks sincerely Prof. A.S. Fokas for arranging the visit to Cambridge University in 2012-2013 and for many useful discussions. KP acknowledges DST, NBHM, CSIR and IFCPAR, Government of India, for the financial support through major projects. RE acknowledges M. K  ray for patient encouragement and is also grateful to NSF, Hungary (OTKA, Ref. No.K83133). This work has been partially supported by The University of Sheffield's MSRC Visitor Grant. We thank editorial board member for his/her suggestions on our submission which has improved the clarity of the paper.

REFERENCES

- [1] G.P. Agrawal, *"Nonlinear Fiber Optics"*, 5th edition (Academic Press, San Diego, CA, 2012).
- [2] B.A.Malomed, *"Soliton management in periodic systems"*(Springer,New Yrok, 2006)
- [3] S.K. Turitsyn, B.G.Bale, M.P.Fedoruk, Phys.Report**521**(2012)135.
- [4] D. J. Korteweg, and G. de Vries, Phil. Mag. **39**(1895)422 .
- [5] N. J. Zabusky and M. D. Kruskal, Phys. Rev. Lett. **15**(1965)240.
- [6] V.E Zakharov and A.B Shabat, Sov. Phys. JETP **34**(1972)62.
- [7] L. F. Mollenauer, R. H. Stolen, and J. P. Gordon, Phys.Rev.Lett. **45**(1980)1095.
- [8] A Hasegawa and F D Tappert, Appl. Phys. Lett. **23**(1973)142 .
- [9] D.H. Peregrine, J. Austral. Math. Soc. B **25**(1983)16.
- [10] D. R. Solli, C. Ropers, P. Koonath,B. Jalali, Nature(London) **450**(2007)1054.
- [11] D. R. Solli, C. Ropers, B. Jalali, Phys. Rev. Lett. **101**(2008) 233902.
- [12] J. M. Dudley, G. Genty and S. Coen, Rev. Mod. Phys. **78**(2006)1135; J. M. Dudley, G. Genty, F. Dias, B. Kibler, N. Akhmediev, Opt. Express **17** (2009) 21497.
- [13] A. N. Ganshin, V. B. Efimov, G.V. Kolmakov, L. P. Mezhov-Deglin, P.V. E. McClintock, Phys.Rev.Lett. **101**(2008)065303.
- [14] Yu. V. Bludov, V. V. Konotop,N. Akhmediev,Phys.Rev.A.**80**(2009)033610.
- [15] M.S. Ruderman,Eur. Phys. J. Special Topics **185**(2010) 57.

- [16] W.M.Moslem, P.K.Shukla, B.Eliasson, Euro. Phys. Lett. **96**(2011)25002.
- [17] R. Höhmann, U. Kuh, H.-J. Stockmann, L. Kaplan, E. J. Heller, Phys.Rev.Lett.**104**(2010)093901.
- [18] M. Shats, H. Punzmann, H. Xia,Phys.Rev.Lett. **104**(2010)104503.
- [19] S.Vergeles,S.K.Turitsyn, Phys.Rev.E **83**(2011)061801(R).
- [20] F. T. Arecchi, U. Bortolozzo, A. Montina, S. Residori, Phys.Rev.Lett.**106**(2011)153901
- [21] A.Chabchoub, N.P.Hoffmann, N.Akhmediev, Phys. Rev. Lett. **106**(2011)204502; J. Geophys. Res. **117**(2012)C00J02.
- [22] B. Kibler, J. Fatome, C. Finot, G. Millot, F. Dias, G. Genty, N. Akhmediev,J. M. Dudley, Nature Phys.**6**(2010)790.
- [23] N. Akhmediev, A. Ankiewicz, M. Taki,Phys. Lett. A**373**(2009)675.
- [24] A. Ankiewicz, J. M. Soto-Crespo, N. Akhmediev, Phys. Rev. E. **81**(2010)046602.
- [25] J. M. Soto-Crespo, Ph. Grelu, N. Akhmediev, Phys.Rev. E **84**(2011)016604.
- [26] A.Ankiewicz, N.Akhmediev, J. M. Soto-Crespo, Phys. Rev. E. **82**(2010)026602.
- [27] U. Bandelow, N. Akhmediev , Phys. Rev. E **86**(2012)026606.
- [28] P. Dubard, V.B. Matveev, Nat. Hazards. Earth. Syst. Sci. **11**(2011)667.
- [29] Y. Ohta, J. K. Yang, Proc. R. Soc. A **468**(2012)1716-1740; Phys.Rev.E **86**(2012)036604.
- [30] S.W.Xu, J.S. He, L.H.Wang, J. Phys. A **44** (2011) 305203; Y.Y.Wang, J.S.He,Y.S. Li, Commun.Theor. Phys. **56** (2011) 995-104; Y.S.Tao ,J.S. He, Phys. Rev. E. **85** (2012) 026601; S.W.Xu, J.S.He,J. Math. Phys. **53** (2012) 063507; J.S.He, S.W.Xu, K. Porsezian, J. Phys. Soc. Jpn. **81** (2012) 124007; J.S. He, S.W. Xu, K. Porsezian, J. Phys. Soc. Jpn. **81** (2012) 033002; S. W. Xu, J. S. He, L. H. Wang, Euro. Phys. Lett. **97** (2012) 30007; J.S.He, S. W.Xu, K. Porsezian, Phys.Rev.E **86**(2012)066603; C.Z.Li, J.S.He, K.Porsezian, Phys.Rev.E **87**(2013)012913; L. H. Wang, K. Porsezian,J. S. He, Phys.Rev.E **87**(2013)053202; S.W. Xu, K. Porsezian, J. S. He, Y. Cheng, Phys.Rev.E **88**(2013)062925.
- [31] G.G.Yang, L.Li, S.T.Jia, Phys.Rev.E **88** (2012) 046608.
- [32] B.L.Guo, L.M.Lin,Chin.Phys.Lett.**28** (2011) 110202.
- [33] F. Baronio, A. Degasperis, M. Conforti, S. Wabnitz, Phys.Rev.Lett. **109**(2012) 044102.
- [34] Z.Y. Qin, M.Gu, Phys.Rev.E **86** (2012) 036601.
- [35] L.C.Zhao, J. Liu, Phys. Rev.E **87** (2013)013201.
- [36] M.Taki,A.Mussot, A. Kudlinski, E. Louvergneaux, M. Kolobov, M. Douay, Phys. Lett.A **374**(2010)691.
- [37] S.H.Chen, L.Y.Song, Phys.Rev.E **87**(2013)032910.
- [38] Q.L.Zha, Phys.Scr.**87**(2013)065401.
- [39] L. J. Li, Z. W. Wu, L. H. Wang, J. S. He, Annals of Physics **334**(2013)198.
- [40] J.S.He, H.R. Zhang, L.H. Wang, K. Porsezian,A.S.Fokas,Phys.Rev.E **87**(2013)052914.
- [41] M.J. Ablowitz and P.A. Clarkson, *“Solitons, Nonlinear Evolution Equations and Inverse Scattering”* (Cambridge University Press, Cambridge, NY, 1991).
- [42] H.Lebland,H.Triki,F.Sanchez and D.Mihalache, Optics Communications **285**(2012)356.
- [43] H.Lebland and D.Mihalache, Romanian Reports in Physics **63**(2011)1254.
- [44] G. Neugebauer and R. Meinel, Phys. Lett. A. **100** (1984)467.
- [45] Y. S. Li, X. S. Gu, M. R. Zou, Acta Mathematica Sinica (New Series) **3**(1985)143.
- [46] V. B. Matveev, M. A. Salle,Darboux transformations and solitons(Springer, Berlin,1991)
- [47] C. H. Gu, Z. X. Zhou, Lett. Math. Phys. **13**(1987)179.
- [48] C. H. Gu, H. S. Hu and Z. X. Zhou, Darboux Trasformations in Integrable Systems (Dortrecht: Springer)(2006).
- [49] J. S. He, L. Zhang, Y. Cheng and Y. S. Li, Science in China Series A: Mathematics. **12**(2006)1867.
- [50] D. J. Kedziora, A. Ankiewicz, and N. Akhmediev, Phys. Rev. E **84**(2011)056611.

TABLE 1. Distribution of peaks on rings by non-standard decomposition

Order	Distributions of peaks on rings (L=Left,R=Right)			
4	5+5(Fig.12)			
5	7+7+1(Fig.13L)	5+5+5(Fig.13R)		
6	9+9+3(Fig.14R)	5+10+5+1(Fig.15L)	7+7+7(Fig.15R)	11+5+5(Fig.16)

Appendix A: In eq.(28), L_1 are L_2 are given by

$$\begin{aligned}
B := & 2239488a^4c^{14}t^6 + 46656a^{12}c^6t^6 + 2985984c^{18}t^6 + 559872a^8c^{10}t^6 \\
& + 746496a^6c^{10}t^5x + 93312a^{10}c^6t^5x - 1492992a^4c^{12}t^5x - 186624a^8c^8t^5x \\
& + 1492992a^2c^{14}t^5x - 2985984c^{16}t^5x + 1244160c^{14}t^4x^2 - 248832a^6c^8t^4x^2 \\
& - 995328a^2c^{12}t^4x^2 + 622080a^4c^{10}t^4x^2 + 77760a^8c^6t^4x^2 - 276480c^{12}t^3x^3 \\
& + 34560a^6c^6t^3x^3 - 124416a^4c^8t^3x^3 + 248832a^2c^{10}t^3x^3 + 34560c^{10}t^2x^4 \\
& + 8640a^4c^6t^2x^4 - 27648a^2c^8t^2x^4 + 1152a^2c^6tx^5 - 2304c^8tx^5 + 64c^6x^6 \\
& - 331776c^6a^6t^4 - 518400c^{12}t^4 + 155520c^8a^4t^4 - 11664c^4a^8t^4 + 290304c^{10}t^3x \\
& - 15552c^4a^6t^3x + 103680c^8a^2t^3x - 176256c^6a^4t^3x - 58752c^8t^2x^2 - 6912c^6a^2t^2x^2 \\
& - 7776c^4a^4t^2x^2 + 4992c^6tx^3 - 1728c^4a^2tx^3 - 144c^4x^4 + 124416ac^{10}s_1t^3 \\
& + 31104a^5c^6s_1t^3 - 165888a^3c^8s_1t^3 + 20736a^3c^6s_1t^2x - 41472ac^8s_1t^2x \\
& + 3456ac^6s_1tx^2 - 18000c^6t^2 - 1620c^2a^4t^2 - 1080c^2a^2tx + 5616c^4tx - 180c^2x^2 \\
& + 864c^4as_1t + 144c^4s_1^2 + 45 + i(2985984ac^{14}t^5 + 1492992a^5c^{10}t^5 \\
& + 186624a^9c^6t^5 - 497664a^5c^8t^4x + 995328a^3c^{10}t^4x - 1990656ac^{12}t^4x \\
& + 248832a^7c^6t^4x - 331776a^3c^8t^3x^2 + 124416a^5c^6t^3x^2 + 497664ac^{10}t^3x^2 \\
& - 55296ac^8t^2x^3 + 27648a^3c^6t^2x^3 + 2304ac^6tx^4 + 207360c^8at^3 - 31104c^4a^5t^3 \\
& - 13824c^6at^2x - 20736c^4a^3t^2x - 3456c^4atx^2 + 20736c^8s_1t^2 - 41472a^2c^6s_1t^2 \\
& + 5184a^4c^4s_1t^2 + 3456a^2c^4s_1tx - 6912c^6s_1tx + 576c^4s_1x^2 - 2160ac^2t + 144s_1c^2)
\end{aligned}$$

and

$$\begin{aligned}
C := & 2239488a^4c^{14}t^6 + 2985984c^{18}t^6 + 46656a^{12}c^6t^6 + 559872a^8c^{10}t^6 \\
& + 746496a^6c^{10}t^5x - 1492992a^4c^{12}t^5x - 186624a^8c^8t^5x - 2985984c^{16}t^5x \\
& + 93312a^{10}c^6t^5x + 1492992a^2c^{14}t^5x + 1244160c^{14}t^4x^2 - 995328a^2c^{12}t^4x^2 \\
& + 622080a^4c^{10}t^4x^2 + 77760a^8c^6t^4x^2 - 248832a^6c^8t^4x^2 + 248832a^2c^{10}t^3x^3 \\
& + 34560a^6c^6t^3x^3 - 124416a^4c^8t^3x^3 - 276480c^{12}t^3x^3 - 27648a^2c^8t^2x^4 \\
& + 8640a^4c^6t^2x^4 + 34560c^{10}t^2x^4 - 2304c^8tx^5 + 1152a^2c^6tx^5 + 64c^6x^6 \\
& + 995328c^{10}a^2t^4 + 279936c^8a^4t^4 - 82944c^6a^6t^4 + 3888c^4a^8t^4 - 269568c^{12}t^4 \\
& + 124416c^{10}t^3x + 5184c^4a^6t^3x - 51840c^6a^4t^3x - 145152c^8a^2t^3x \\
& - 17280c^8t^2x^2 - 6912c^6a^2t^2x^2 + 2592c^4a^4t^2x^2 + 384c^6tx^3 \\
& + 576c^4a^2tx^3 + 48c^4x^4 - 165888a^3c^8s_1t^3 + 124416ac^{10}s_1t^3 \\
& + 31104a^5c^6s_1t^3 + 20736a^3c^6s_1t^2x - 41472ac^8s_1t^2x + 3456ac^6s_1tx^2 \\
& + 20016c^6t^2 + 972c^2a^4t^2 + 6912c^4a^2t^2 + 648c^2a^2tx - 2448c^4tx + 108c^2x^2 \\
& - 2592c^4as_1t + 144c^4s_1^2 + 9.
\end{aligned}$$

Appendix B: In eq.(29), L_1 are L_2 are given by

$$\begin{aligned}
L_1 := & -4939273445868140625t^{12} - 545023276785450000t^{11}x - 388407392651700000t^{10}x^2 \\
& - 34025850934560000t^9x^3 - 12374529519456000t^8x^4 - 841946352721920t^7x^5 \\
& - 204871837925376t^6x^6 - 10322713903104t^5x^7 - 1860148592640t^4x^8 - 62710087680t^3x^9
\end{aligned}$$

$$\begin{aligned}
& -8776581120t^2x^{10} - 150994944tx^{11} - 16777216x^{12} + 2300237292280725000t^{10} \\
& + 500080291038360000t^9x + 178207653254544000t^8x^2 + 20160748631347200t^7x^3 \\
& + 4231975119851520t^6x^4 + 253682249269248t^5x^5 + 40317552230400t^4x^6 + 880347709440t^3x^7 \\
& + 141203865600t^2x^8 - 1447034880tx^9 + 75497472x^{10} + 257120426548112400t^8 \\
& - 88521031030049280t^7x - 1841385225323520t^6x^2 - 617799343104000t^5x^3 \\
& - 88747774156800t^4x^4 - 8252622766080t^3x^5 - 200693514240t^2x^6 + 1415577600tx^7 \\
& + 235929600x^8 + 12647412412496640t^6 + 42148769126400t^5x - 2996161228800t^4x^2 \\
& - 15902996889600t^3x^3 + 313860096000t^2x^4 - 8139571200tx^5 + 707788800x^6 \\
& - 149676507590400t^4 + 2148738969600t^3x - 1622998425600t^2x^2 + 31186944000t^3x \\
& - 928972800x^4 - 95215564800t^2 + 21598617600tx - 464486400x^2 + 58060800 \\
& + i(-6540279321425400000t^{11} - 601404995073600000t^{10}x - 423057306879360000t^9x^2 \\
& - 29901007761408000t^8x^3 - 10648770814771200t^7x^4 - 552411244265472t^6x^5 \\
& - 130559642173440t^5x^6 - 4494741995520t^4x^7 - 779700142080t^3x^8 - 13589544960t^2x^9 \\
& - 1811939328tx^{10} - 303419904173280000t^9 + 263517097430016000t^8x \\
& + 29562711599923200t^7x^2 + 7820253397647360t^6x^3 + 799710056939520t^5x^4 \\
& + 58500443013120t^4x^5 + 5243865661440t^3x^6 + 40768634880t^2x^7 + 6794772480tx^8 \\
& + 10822374648023040t^7 - 15805156998758400t^6x - 366298181959680t^5x^2 \\
& + 157459297075200t^4x^3 - 6736379904000t^3x^4 - 249707888640t^2x^5 + 16986931200tx^6 \\
& + 2321279745269760t^5 - 164322282700800t^4x + 7849554739200t^3x^2 - 700710912000t^2x^3 \\
& + 38220595200tx^4 + 4992863846400t^3 - 967458816000t^2x - 33443020800tx^2 - 8360755200t) \\
L_2 := & 4939273445868140625t^{12} + 545023276785450000t^{11}x + 388407392651700000t^{10}x^2 \\
& + 34025850934560000t^9x^3 + 12374529519456000t^8x^4 + 841946352721920t^7x^5 \\
& + 204871837925376t^6x^6 + 10322713903104t^5x^7 + 1860148592640t^4x^8 \\
& + 62710087680t^3x^9 + 8776581120t^2x^{10} + 150994944tx^{11} + 16777216x^{12} \\
& + 1671541529351175000t^{10} - 201221180459640000t^9x + 29583374214960000t^8x^2 \\
& - 8646206984294400t^7x^3 - 205872145551360t^6x^4 - 102185078390784t^5x^5 \\
& - 5361951375360t^4x^6 - 141416202240t^3x^7 - 16349921280t^2x^8 + 2202009600tx^9 \\
& + 25165824x^{10} + 214192109547903600t^8 + 4346367735790080t^7x \\
& + 3783154346910720t^6x^2 - 1075635551969280t^5x^3 + 40942170316800t^4x^4 \\
& + 1840480911360t^3x^5 + 84333035520t^2x^6 + 849346560tx^7 + 141557760x^8 \\
& + 3537485306138880t^6 + 789853361080320t^5x + 130057245388800t^4x^2 \\
& - 11222478028800t^3x^3 + 402245222400t^2x^4 - 4034396160tx^5 + 613416960x^6 \\
& + 90779142700800t^4 - 6216180019200t^3x - 269186457600t^2x^2 + 11988172800tx^3 \\
& + 221184000x^4 + 213178521600t^2 - 5009817600tx + 199065600x^2 + 8294400.
\end{aligned}$$

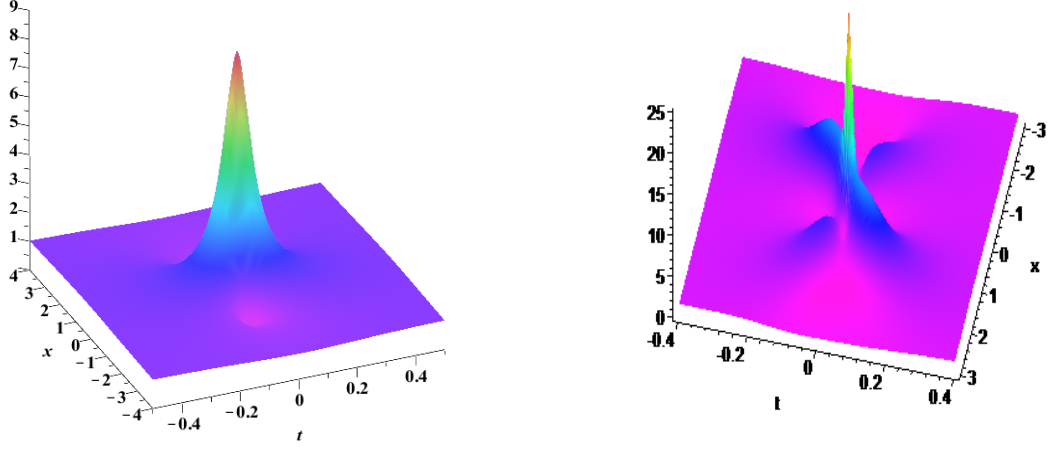


Figure 1. (Color online) Fundamental pattern of the rogue wave. (a) The left figure is the evolution of $|q^{[1]}|^2$ (**1st-order** rogue wave) with specific parameters $a = 1.5, c = 1, s_0 = 0$. (b) The right figure is $|q^{[2]}|^2$ (**2nd-order** rogue wave) with specific parameters $a = 1.44, c = 1, s_0 = 0, s_1 = 0$.

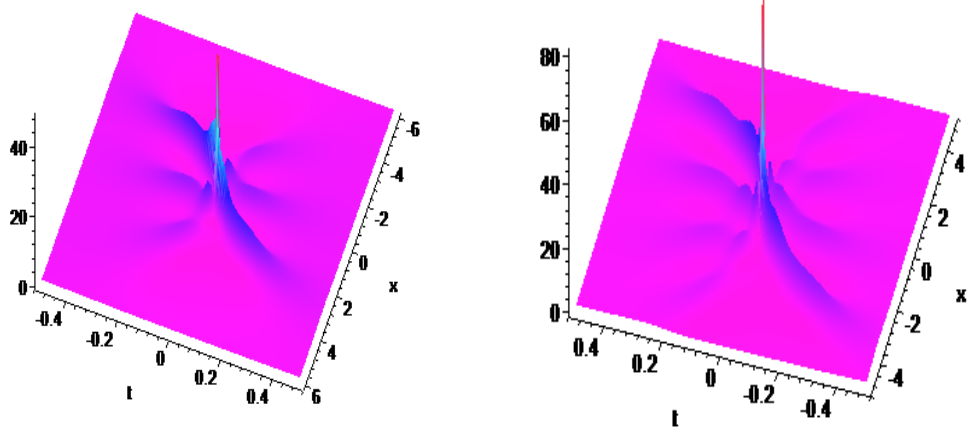


Figure 2. (Color online) Fundamental pattern of the rogue wave. (a) The left figure is the evolution of $|q^{[3]}|^2$ (**3rd-order** rogue wave) with specific parameters $a = 1.4, c = 1, s_0 = 0, s_1 = 0, s_2 = 0$. (b) The right figure is $|q^{[4]}|^2$ (**4th-order** rogue wave) with specific parameters $a = 1.48, c = 1, s_0 = 0, s_1 = 0, s_2 = 0, s_3 = 0$.

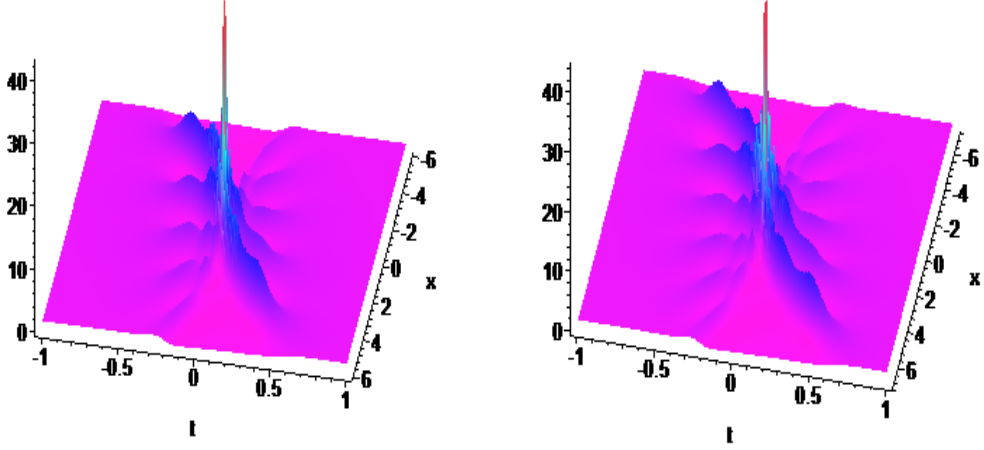


Figure 3. (Color online) Fundamental patterns of the rogue waves. (a) The left figure is the evolution of $|q^{[5]}|^2$ (**5th-order** rogue wave) with specific parameters $a = 1.5, c = 1, s_0 = 0, s_1 = 0, s_2 = 0, s_3 = 0, s_4 = 0$. (b) The right figure is $|q^{[6]}|^2$ (**6th-order** rogue wave) with specific parameters $a = 1.5, c = 1, s_0 = 0, s_1 = 0, s_2 = 0, s_3 = 0, s_4 = 0, s_5 = 0$.

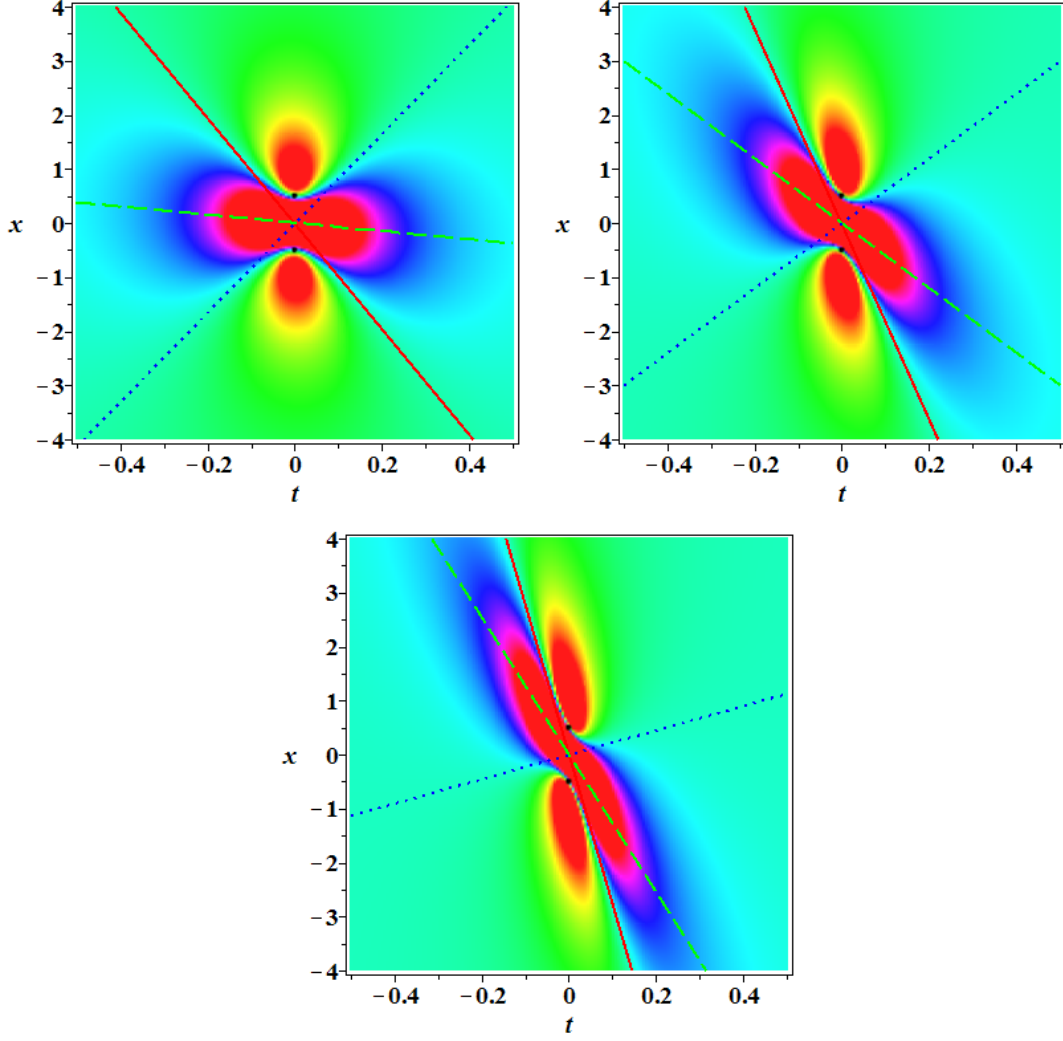


Figure 4. (Color online) The density plots of the first-order rogue wave $|q^{[1]}|^2$ with $c = 1$ and different values of a . From left to right, $a = 1.5, 2, 2.5$ in order. Here red (solid) and blue (dot) lines are plotted for two asymptotes of contour lines at height c^2 , green (dash) line is plotted for a median of one triangle composed of above two asymptotes and a parallel line of x -axis except $t = 0$. Two fixed points are located at $(0, 0.5)$ and $(0, -0.5)$ in three panels.

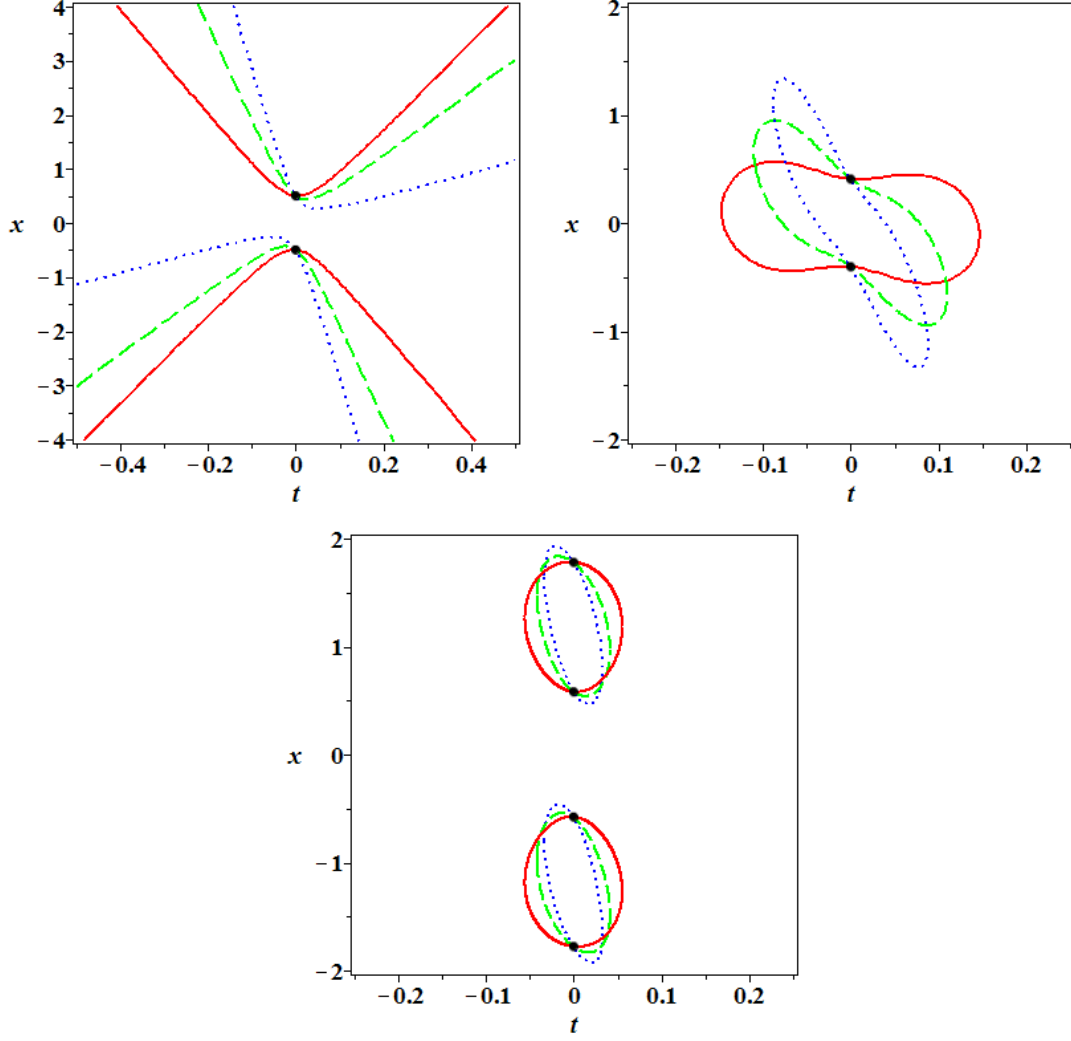


Figure 5. (Color online) Contour lines of the first-order rogue wave with $c = 1$ and $a = 1.5$ (red, solid), 2 (dash, green), 2.5 (dot, blue). From left to right, panels are plotted for contour lines of $|q^{[1]}|^2$ at height c^2 (on asymptotic plane), $c^2 + 1$, $c^2/2$ in order. There are fixed points located at $(0, 0.50)$ and $(0, -0.50)$ in the left panel, $(0, 0.41)$ and $(0, -0.41)$ in the middle panel, $(0, 1.78)$ and $(0, 0.58)$, $(0, -0.58)$ and $(0, -1.78)$ in the right panel.

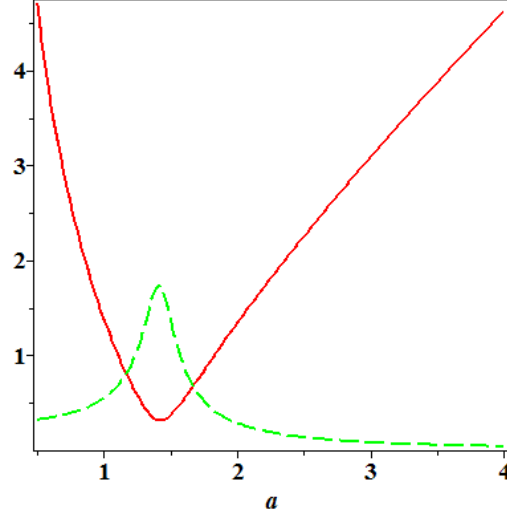


Figure 6. (Color online) The length (red, solid) and the width (dash, green) of the first-order RW $|q^{[1]}|^2$ with fixed $c = 1$. Note $a = \sqrt{2}$ is an extreme point of d_L and d_W .

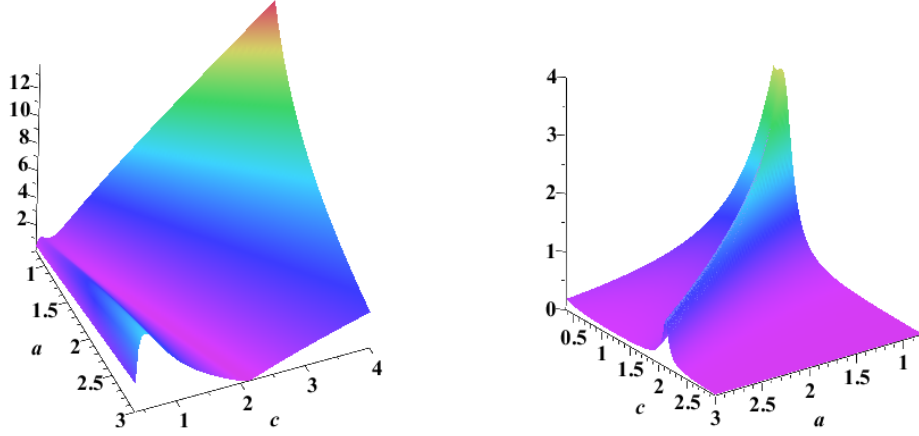


Figure 7. (Color online) The length(left) and width(right) of the first-order RW $|q^{[1]}|^2$ with two parameters a and c .

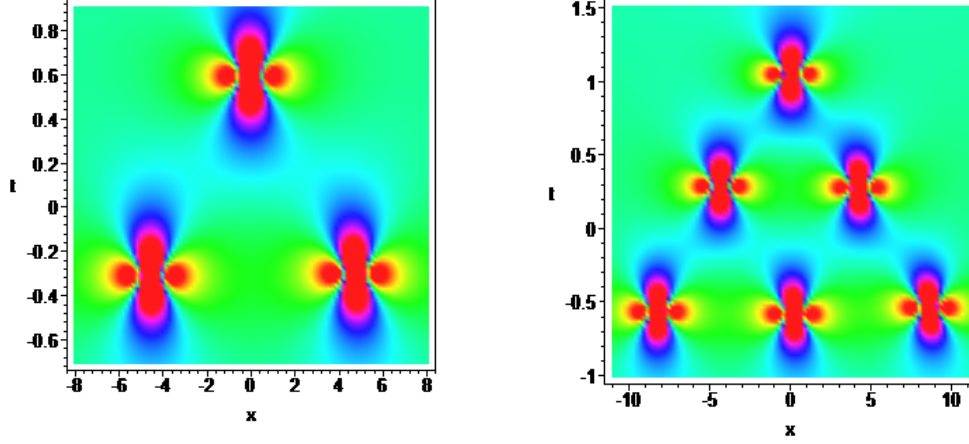


Figure 8. (Color online) Triangular pattern of the 2nd- and 3rd-order rogue waves. The left panel is a density plot of $|q^{[2]}|^2$ (**2nd-order** rogue wave) with $a = 1.44, c = 1, s_0 = 0, s_1 = 100$. The right panel is a density plot of $|q^{[3]}|^2$ (**3rd-order** rogue wave) with $a = 1.44, c = 1, s_0 = 0, s_1 = 100, s_2 = 0$.

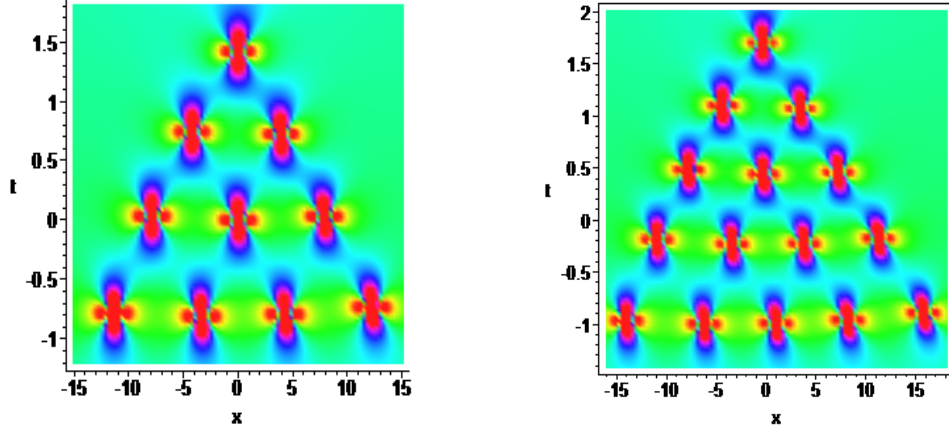


Figure 9. (Color online) Triangular pattern of the 4th-order and 5th-order rogue waves. The left panel is a density plot of $|q^{[4]}|^2$ (**4th-order** rogue wave) with $a = 1.46, c = 1, s_0 = 0, s_1 = 100, s_2 = 0, s_3 = 0$, the right panel is a density plot of $|q^{[5]}|^2$ (**5th-order** rogue wave) with $a = 1.5, c = 1, s_0 = 0, s_1 = 100, s_2 = 0, s_3 = 0, s_4 = 0$.

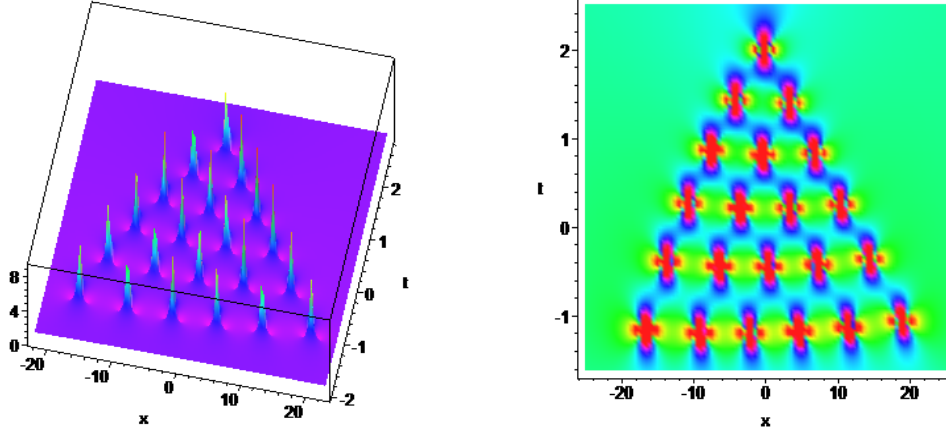


Figure 10. (Color online) Triangular pattern of the 6th-order rogue wave. (a) The left figure is the evolution of $|q^{[6]}|^2$ (**6th-order** rogue wave) and (b) the right figure is the corresponding density plot with $a = 1.5, c = 1, s_0 = 0, s_1 = 100, s_2 = 0, s_3 = 0, s_4 = 0, s_5 = 0$.

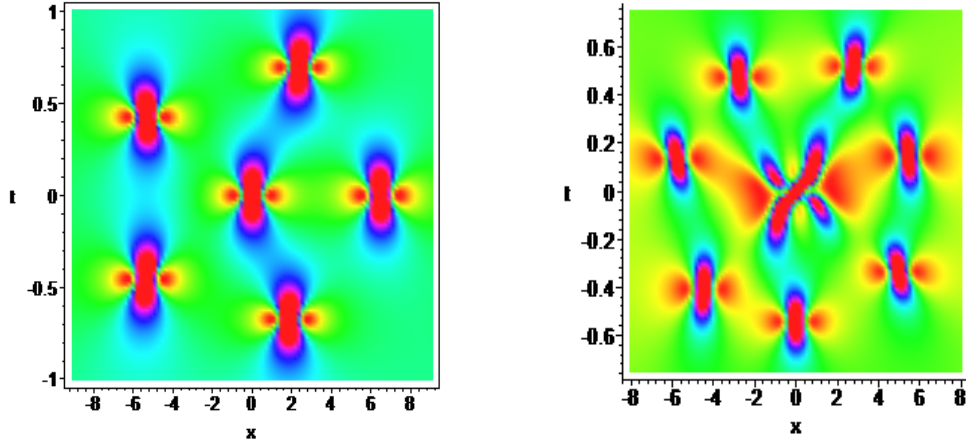


Figure 11. (Color online) Standard circular decomposition of the rogue wave: inner peak surrounded by ring pattern. The left panel is a density plot of $|q^{[3]}|^2$ (**3rd-order** rogue wave) with $a = 1.4, c = 1, s_0 = 0, s_1 = 0, s_2 = 1000$, the right panel is a density plot of $|q^{[4]}|^2$ (**4th-order** rogue wave) with $a = 1.48, c = 1, s_0 = 0, s_1 = 0, s_2 = 0, s_3 = 1000$.

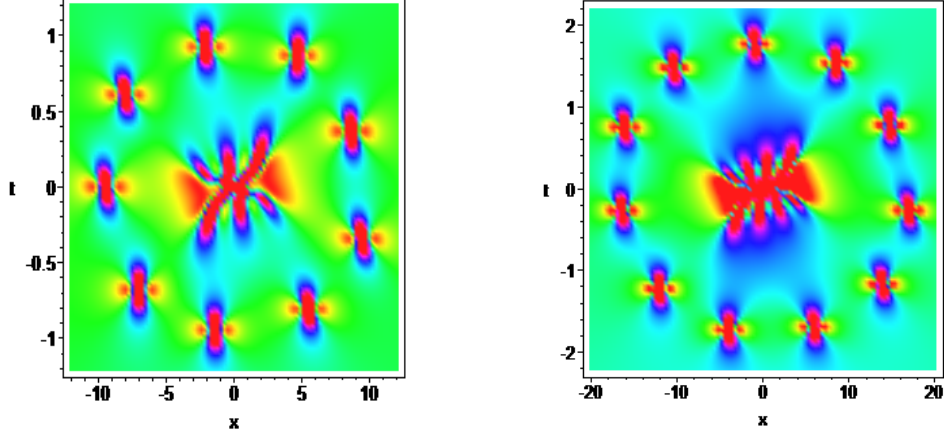


Figure 12. (Color online) Standard circular decomposition of the rogue wave: a ring pattern with inner 3rd (left) and 4th (right) fundamental patterns. The left panel is a density plot of $|q^{[5]}|^2$ (**5th-order** rogue wave) with $a = 1.5, c = 1, s_0 = 0, s_1 = 0, s_2 = 0, s_3 = 0, s_4 = 100000$, the right panel is a density plot of $|q^{[6]}|^2$ (**6th-order** rogue wave) with $a = 1.5, c = 1, s_0 = 0, s_1 = 0, s_2 = 0, s_3 = 0, s_4 = 0, s_5 = 100000000$.

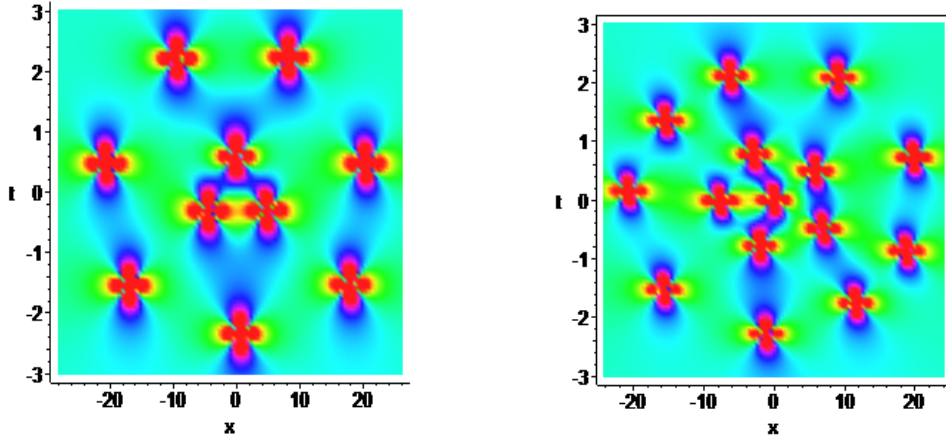


Figure 13. (Color online) Standard circular decomposition of the 4th and 5th rogue waves. The left panel is a density plot of $|q^{[4]}|^2$ (**4th-order** rogue wave) with $a = 1.45, c = 1, s_0 = 0, s_1 = 100, s_2 = 0, s_3 = 10000000$ which is decomposed into an outer ring with an inner 2nd triangular pattern, the right panel is a density plot of $|q^{[5]}|^2$ (**5th-order** rogue wave) with $a = 1.5, c = 1, s_0 = 0, s_1 = 100, s_2 = 0, s_3 = 500000, s_4 = 100000000$ which is decomposed into an inner peak surrounded by two rings.

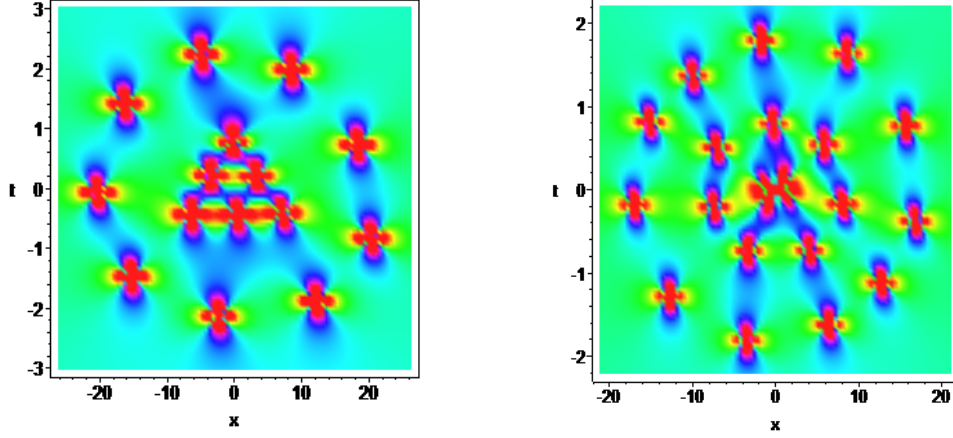


Figure 14. (Color online) Standard circular decomposition of the 5th and 6th rogue waves. The left panel is a density plot of $|q^{[5]}|^2$ (**5th-order** rogue wave) with $a = 1.5, c = 1, s_0 = 0, s_1 = 50, s_2 = 0, s_3 = 0, s_4 = 100000000$ which is decomposed into a ring pattern with an inner 3rd triangular pattern, the right panel is a density plot of $|q^{[6]}|^2$ (**6th-order** rogue wave) with $a = 1.5, c = 1, s_0 = 0, s_1 = 0, s_2 = 0, s_3 = 0, s_4 = 1000000, s_5 = 100000000$ which is decomposed into two ring patterns plus an inner 2nd fundamental pattern.

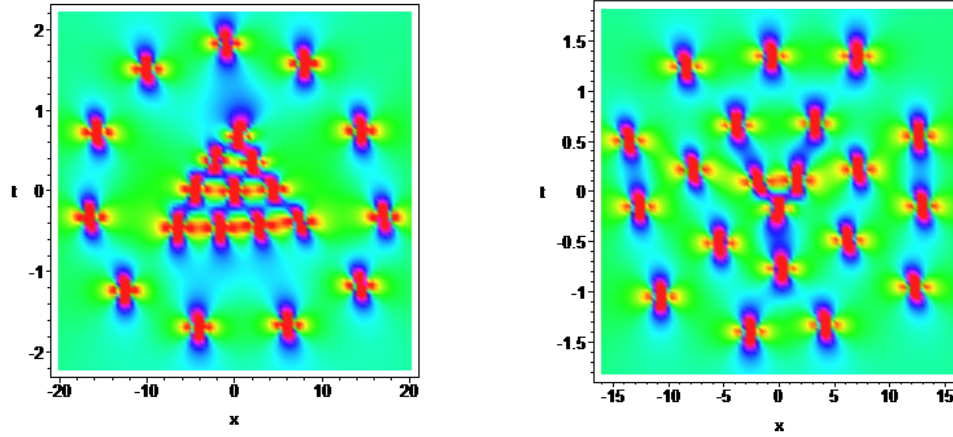


Figure 15. (Color online) Standard circular decomposition of the 6th rogue wave. The left panel is a density plot of $|q^{[6]}|^2$ (**6th-order** rogue wave) with $a = 1.5, c = 1, s_0 = 0, s_1 = 18, s_2 = 0, s_3 = 0, s_4 = 0, s_5 = 100000000$ which is decomposed into a ring plus an inner 4th triangular pattern, the right panel is a density plot of $|q^{[6]}|^2$ (**6th-order** rogue wave) with $a = 1.5, c = 1, s_0 = 0, s_1 = 0, s_2 = 0, s_3 = 7000, s_4 = 0, s_5 = 10000000$ which is decomposed into three rings.

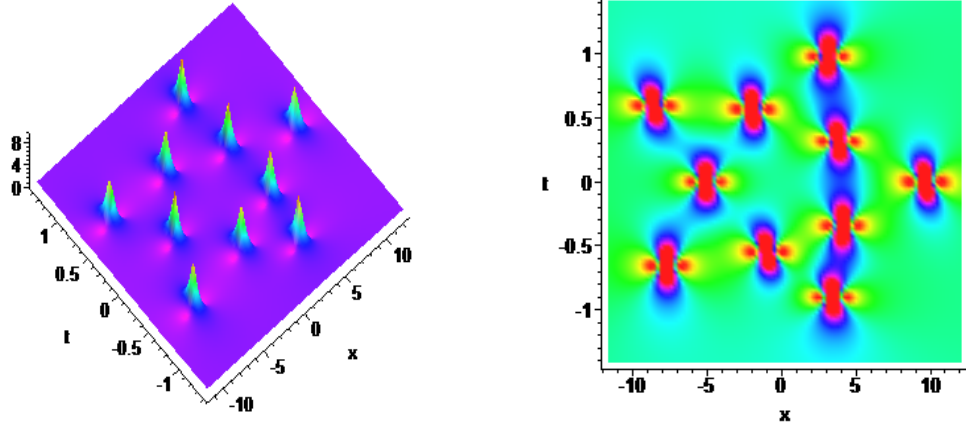


Figure 16. (Color online) Non-standard circular decomposition of the 4th-rogue wave: two rings. (a) The left figure is the dynamical evolution of $|q^{[4]}|^2$ (**4th-order** rogue wave) and (b) the right figure is the corresponding density plot with $a = 1.48, c = 1, s_0 = 0, s_1 = 0, s_2 = 1000, s_3 = 0$.

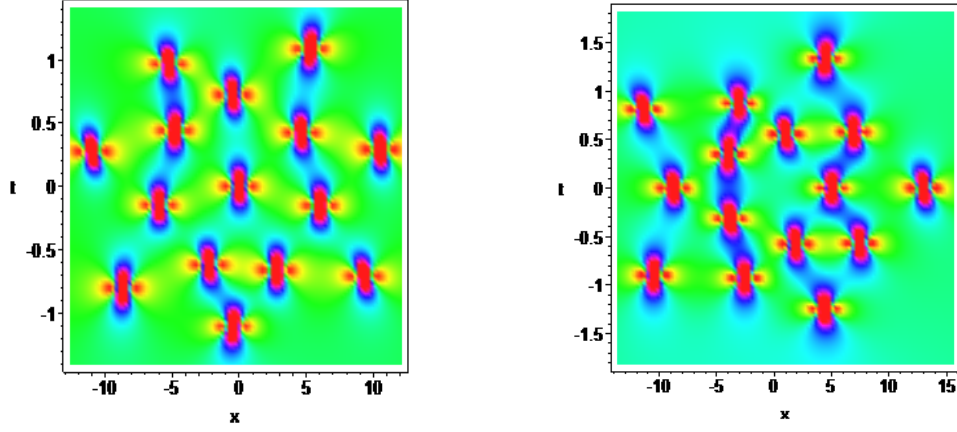


Figure 17. (Color online) Non-standard circular decomposition of the 5th-rogue waves: two rings plus an inner peak (left) and three rings (right). The left panel is a density plot of $|q^{[5]}|^2$ (**5th-order** rogue wave) with $a = 1.45, c = 1, s_0 = 0, s_1 = 0, s_2 = 0, s_3 = 10000, s_4 = 0$, the right panel is a density plot of $|q^{[5]}|^2$ (**5th-order** rogue wave) with $a = 1.46, c = 1, s_0 = 0, s_1 = 0, s_2 = 1000, s_3 = 0, s_4 = 0$.

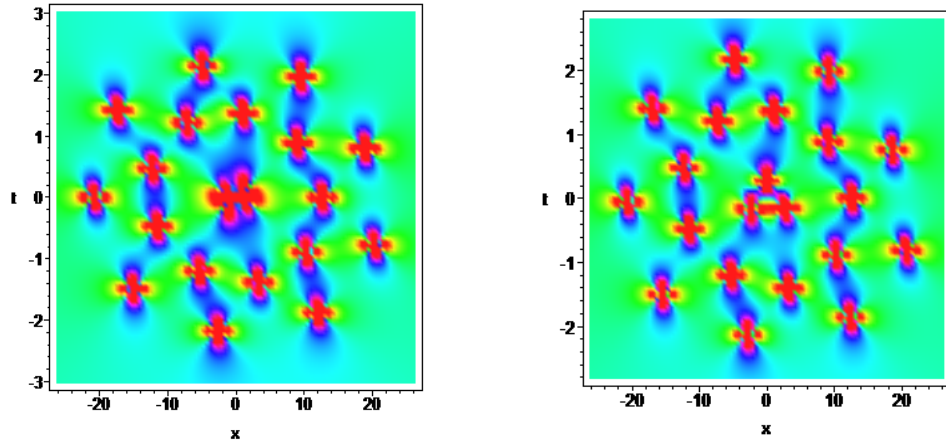


Figure 18. (Color online) Non-standard circular decomposition of the 6th-rogue wave: two ring patterns with an inner 2nd fundamental pattern(left) and three rings(right). The left panel is a density plot of $|q^{[6]}|^2$ (**6th-order** rogue wave) with $a = 1.5, c = 1, s_0 = 0, s_1 = 0, s_2 = 0, s_3 = 0, s_4 = 10000000, s_5 = 0$, the right panel is a density plot of $|q^{[6]}|^2$ (**6th-order** rogue wave) with $a = 1.5, c = 1, s_0 = 0, s_1 = 15, s_2 = 0, s_3 = 0, s_4 = 10000000, s_5 = 0$.

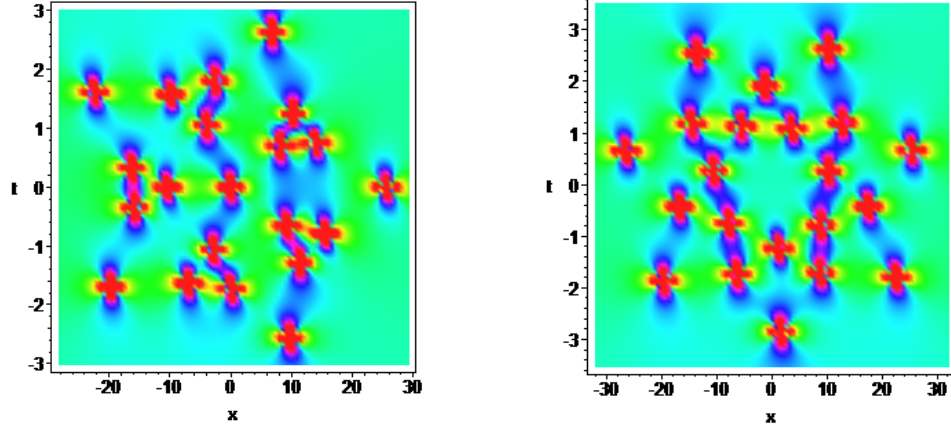


Figure 19. (Color online) Non-standard circular decomposition of the 6th-rogue wave: three rings plus an inner peak (left) and three rings (right). The left panel is a density plot of $|q^{[6]}|^2$ (**6th-order** rogue wave) with $a = 1.5, c = 1, s_0 = 0, s_1 = 0, s_2 = 10000, s_3 = 0, s_4 = 0, s_5 = 0$, the right panel is a density plot of $|q^{[6]}|^2$ (**6th-order** rogue wave) with $a = 1.5, c = 1, s_0 = 0, s_1 = 0, s_2 = 0, s_3 = 1000000, s_4 = 0, s_5 = 100000000$.

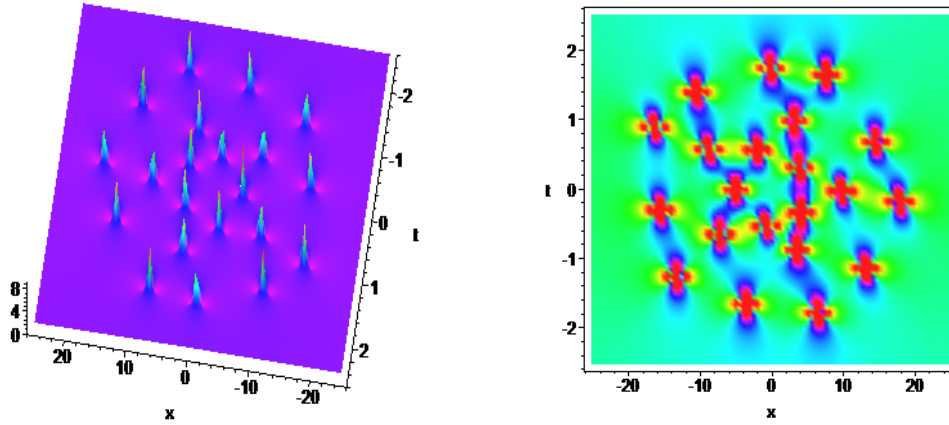


Figure 20. (Color online) Non-standard circular decomposition of the 6th-rogue wave: three rings. (a) The left panel is the dynamical evolution of $|q^{[6]}|^2$ (**6th-order** rogue wave) and (b) the right panel is the corresponding density plot with $a = 1.5, c = 1, s_0 = 0, s_1 = 0, s_2 = 1000, s_3 = 1000000, s_4 = 0, s_5 = 100000000$.

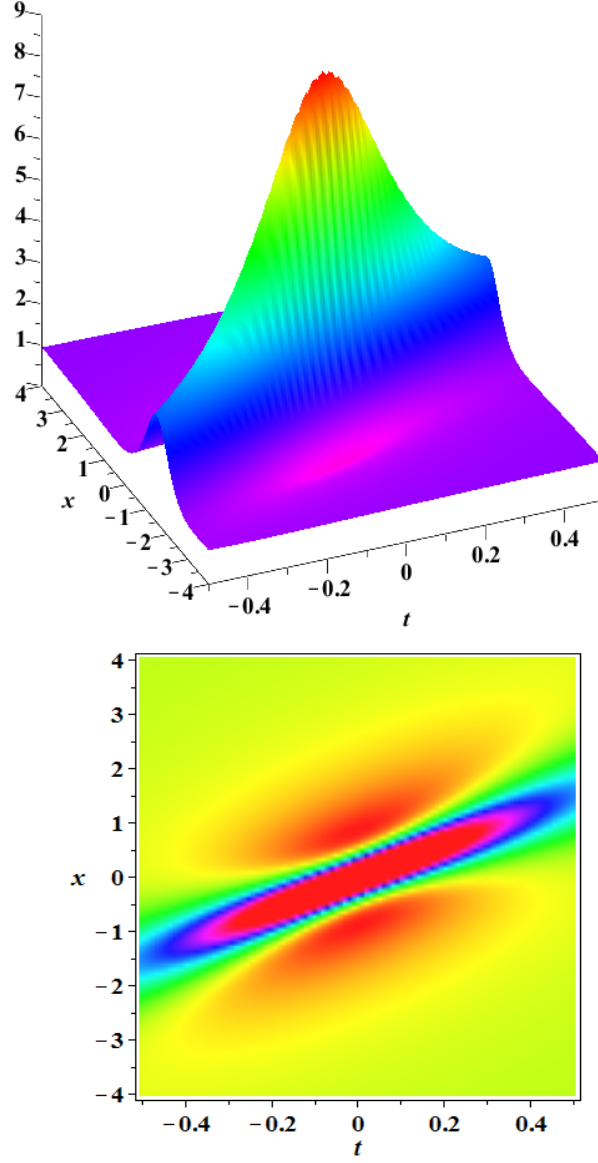


Figure 21. (Color online) The first-order rogue wave ($|q_{NLS}^{[1]}|^2$) of the NLS with $a = 1.5$ and $c = 1$. The left panel is the dynamical evolution of $|q_{NLS}^{[1]}|^2$ and the right panel is the corresponding density plot.

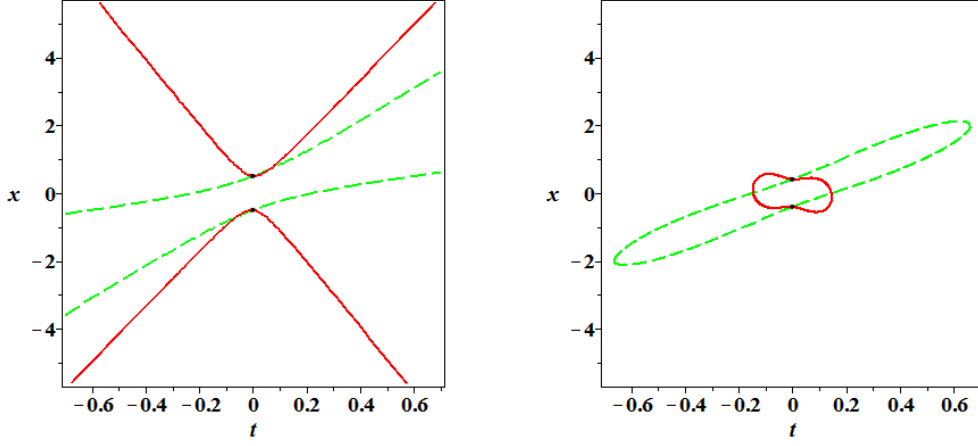


Figure 22. (Color online) Contour lines of the first-order rogue wave of the complex mKdV ($|q^{[1]}|^2$, red, solid) and NLS ($|q_{NLS}^{[1]}|^2$, green, dash) with $a = 1.5$ and $c = 1$. The left panel is plotted at height c^2 (on the asymptotical plane), the right panel is plotted at height $c^2 + 1$. Two lines have two common points: $(0, 0.50)$, $(0, -0.50)$ in the left panel and $(0, 0.41)$, $(0, -0.41)$ in the right panel.